EUROPEAN ORGANIZATION FOR NUCLEAR RESEARCH

NP Internal Report 70-10
7 April, 1970

IHEP (SERPUKHOV) - CERN EXPERIMENTS

J.V. Allaby

CERN

Geneva, Switzerland

Invited Paper Presented at the
Conference on Expectations for Particle Reactions at the
New Accelerators, University of Wisconsin, Madison,
March 30, 31 and April 1, 1970.

IHEP (Serpukhov) - CERN Experiments

Introduction

Some years ago, a casual conversation took place between Victor Weisskopf, then the Director General of CERN, and a fellow theoretician Professor A.A. Logunov, who is now the Director of the Institute for High Energy Physics (IHEP), on the subject of the new Russian accelerator then under construction near Serpukhov. Prof. Weisskopf has always been deeply interested in extending contacts between physicists all over the world, independent of their nationality, or politics, and he suggested the possibility of technical help from CERN to aid in the construction of sophisticated beams from the new accelerator. The present collaboration between IHEP and CERN is the direct result of that bold proposal.

The agreement provides that CERN will construct and supervise the installation of a fast ejection system and the separators for an R.F. separated bubble chamber beam which will separate K-mesons and antiprotons up to 36 GeV/c. In return, CERN will obtain some bubble chamber pictures to be taken with this equipment, and has the possibility to have a team of physicists working in collaboration with a Russian group doing counter physics experiments.

The first of these collaborative experiments was completed in Summer 1969 and many of the results have already appeared in the literature[1]. The second will start very soon, around May 1970. In this talk I shall mainly discuss the first experiment, but I shall say a few words about the aims of the second.

Aims of the First Experiment

It is natural when a new accelerator is constructed to include, early in the experimental programme, a survey of the fluxes of various particles produced by the interaction of the protons of the machine with suitable targets; this formed the first part of our joint

experiment. An additional motivation for choosing this measurement was the need to study the techniques necessary for identifying particles (π^-, K^-, $\bar{p}$) in the momentum range up to 65 GeV/c. Such measurements would clearly give valuable data for the design of future experiments. However valuable this may be, it is not too exciting for a group of physicists with their hands on a new machine, so the experiment did not stop there, but included a second part which was to make some measurements of total cross-sections in the new momentum range available, to a precision of about $\pm$ 1%.

It must be stressed that this experiment was limited to negative particles only. Because of the relatively short straight sections, it is rather difficult to produce a positive beam from an internal target and a positive beam did not, and still does not, exist at the IHEP accelerator, although a diffracted proton beam is planned for the future.

Negative Particle Production

This part of the experiment was itself split into two phases. The first phase consisted of measurements in beam 2 which could accept negative particles in the range 40-65 GeV/c. The second phase was a continuation in beam 4 which could accept negative particles in the range 25-40 GeV/c. These ranges are for accelerator operation at 70 GeV. If the accelerator runs at lower energy, these ranges just scale down in proportion since the limitation stems from the orbits through the magnets of the accelerator. Fig. 1 shows the layout of the experimental area.

The measurements of particle production will be described using the set-up of beam 2 as the example of how the experiment was carried out.

Fig. 2 shows the detail of the beam channel 2 as used for the particle production measurements.

The secondary beam channel was designed to accept negative particles of 40, 50 or 60 GeV/c produced at an angle of 0 mrad from one of three targets spaced azimuthally inside a magnet unit of the accelerator. By varying the radial position of these targets, various combinations of momentum and angle could be obtained in the range 40-65 GeV/c and 0-15 mrad. The production angle and momenta of the secondaries from any one target could not be independently varied. The targets were made of aluminium, and were cylindrical with length 21 mm and diameter 2 mm. Two independent monitors, a threefold telescope P and a fourfold telescope F, were aligned on the target to detect charged secondaries.

Collimators K_1 and K_2 defined the beam acceptance vertically and horizontally, respectively. The quadrupole lenses L_1 - L_4 produced a horizontal focus at the momentum slit K_3 which defined the momentum acceptance; L_5 - L_7 produced the parallel part (between L_7 and L_8) and L_9 - L_{10} yielded a final focus in both horizontal and vertical planes at the position of counter S_5. The total beam length to S_5 was 120 m.

The composition of the beam was measured independently by various combinations of Čerenkov counters of different design, in order to gain information on possible difficulties of detection in this new momentum range. This redundancy provided a valuable cross-check of the data. The beam was defined geometrically by scintillation counters A_2 A_3 or S S_2 S_4 S_5. For particle identification the following detectors were available: two chromatically compensated differential Čerenkov counters, D and ⌣ (DISC's); two Čerenkov counters C_1 and C_2, which could be used as either threshold or differential-threshold counters; a final threshold Čerenkov counter C_3, which was frequently used in anti-coincidence. Their positions are indicated in Fig. 2.

The D counter was 2 m long and used CO_2 gas as radiator[2]. The Čerenkov light from the desired particles, after passing through a compensator for chromatism, was detected by nine photomultipliers placed behind a variable aperture annular diaphragm. D_6 consisted of a sixfold coincidence between three pairs of phototubes and three single phototubes. D_9 was a direct ninefold coincidence which gave the best signal-to-noise ratio, but rather small efficiency ($\approx$ 35% with smallest diaphragm opening), resulting from low photoelectron statistics. The efficiency of D_6 was $\approx$ 70%. The Δ counter was 2.5 m long and similar in construction to the D counter. However, it had 12 photomultipliers to detect the Čerenkov light, but with logic very similar to the D counter, enabling an equivalent choice of the order of coincidence demanded. Normally the combination Δ_6 was used with an efficiency in the range of 35 to 70%. Both counters had a resolution of $\Delta\beta \approx 2 \times 10^{-5}$. The refractive index of the gas of both counters was measured with Rayleigh interferometers, one using a visual setting on the achromatic fringe and a visual read-out of the micrometer driving the compensating glass plate, the other using a digital output of the number of fringes obtained in filling the empty refractometer to the counter pressure, using the monochromatic red line of a He - Ne laser.

C_1 and C_2 were 5 m long threshold Čerenkov counters with spherical mirrors and a single photomultiplier, providing a resolution $\Delta\beta = 6.5 \times 10^{-6}$ (where $\Delta\beta$ is defined as the width in β from threshold to 63% efficiency). The counter efficiency on the plateau was better than 99.99%. Nitrogen or helium were the gases used as radiator. The counters could be used in normal threshold mode or in a differential-threshold mode[3]. In the latter case, pulse-height discrimination on the output of the photomultiplier was used to reject large pulses from unwanted particles. The last Čerenkov counter C_3 was 13 m long and used a plane mirror to reflect the Čerenkov light onto a single photomultiplier through a quartz lens. It had a resolution of $\Delta\beta = 7 \times 10^{-6}$.

During the data taking, as many as four independent techniques for the measurement of the composition of the beam were used. The two differential counters, D and Δ, produced independent pressure curves, and two different modes of operation of the threshold counters were employed either using the normal threshold properties of all the counters, or using the counters C_1 and C_2 in the differential-threshold mode.

Typical pressure curves for these four techniques are illustrated in Fig. 3. Fig. 3a is a pressure curve of the D counter. Fig. 3b is a similar curve using the Δ counter. Fig. 3c shows the threshold counter operation. Fig. 3d shows the data obtained using the counters C_1 and C_2 in their differential-threshold mode (denoted by C_1* and C_2*). $\bar{C}_3$ was used to veto the lighter particles when K^- or $\bar{p}$ were detected. The clean separation demonstrated by these curves shows that the identification of π^-, K^-, and $\bar{p}$ up to a momentum of 60 GeV/c can be achieved with only Čerenkov counter techniques.

From pressure curves such as those shown in Fig. 3 the ratios of particles reaching the final scintillation counter could be immediately derived. The particle ratios are directly proportional to the ratios of the areas of the peaks in the pressure curves of the differential Čerenkov counters. For the threshold counter data, the particle ratios were derived from the steps in the curves at the particle thresholds. The particle ratios at the production target were obtained by correcting for decay and absorption. The data obtained by the methods described previously agree within the estimated errors and the final results are a weighted average of these data.

Two methods were used to normalize the flux of secondaries. The first was a measurement of the secondary beam rate normalized to 10^{12} circulating protons as indicated by the internal beam

monitor of the synchroton. The standard collimator size for this measurement was 4 x 4 cm^2 (corresponding to $\Delta\Omega = 8 \times 10^{-6}$ sr from target 2) and the momentum slit K_3 was set to $\pm$ 6 mm corresponding to $\pm$ 1% for $\Delta P/P$. In the second method an absolute calibration giving a cross section scale was obtained from measurements of the ^{22}Na produced in the aluminium targets when exposed to the internal beam for controlled periods. The activation cross-section was assumed to remain constant from 28 to 70 GeV, and a value of 10 mb was used[4]. This method provided an absolute calibration of the two monitors F and P.

The techniques described were used in channel 4 to produce the data in the lower momentum range. In addition a successful measurement was made in channel 4 of the production of anti-deuterons, using both Čerenkov techniques and time-of-flight to identify the antideuteron. Fig. 4 shows the pressure curve taken with the differential Čerenkov counter illustrating the detection of antideuterons at 25.1 GeV/c.

Fig. 5 displays the spectra for π^-, K^-, $\bar{p}$ and $\bar{d}$ produced by 70 GeV proton aluminium collisions. The scale on the left gives the differential cross-section per aluminium nucleus, whilst the scale on the right gives the flux in number of particles per 10^{12} circulating protons into a solid angle $\Delta\Omega = 8 \times 10^{-6}$ sr and momentum bite $\Delta P = 1$ GeV/c. A large error of $\pm$ 50% has been assigned to the absolute cross-sections because of possible systematic error in the normalization described above.

Fig. 6 shows a compilation of the data on the production ratios K^-/π^- and $\bar{p}/\pi^-$. Here data taken at incident energies in the range 20 - 70 GeV are all plotted on one graph as a function of P/P_{max}, where P_{max} is the maximum momentum in the laboratory

of the heavier particle (K^- or $\bar{p}$) assuming the usual conservation laws. The broken curve shows the trend of precise data taken earlier at CERN on p-p collisions at 19.2 GeV/c[5]. The variable P/P_{max} seems useful to extrapolate the particle ratios to higher energies, at least near the upper ends of the momentum spectra. Note that the ratios are not strongly dependent on the production angle.

Total Cross-Section Measurements

These measurements were carried out in beam channel 2. Fig. 7 shows the layout of the beam which was essentially identical with that used for particle production. The parallel section contained one differential Čerenkov counter D, and was followed by a high resolution threshold counter C, both used for particle identification. The final focus was on the first of the transmission counters.

Twelve circular transmission counters with diameters from 6 cm to 40 cm were mounted on a trolley which could move on rails along the beam line, downstream of the targets. At each momentum the trolley was moved such that the solid angle subtended by the sixth transmission counter accepted a fixed range of four-momentum transfer squared, t, namely: $|t| \leq 0.038$ $(GeV/c)^2$. This was done to avoid energy-dependent systematic errors in the extrapolation procedure. At 20 GeV/c and 25 GeV/c the trolley could not be moved far enough forward to fulfil this criterion and thus stayed fixed at the minimum distance from the targets. Two small counters, S_4 and S_5, were also mounted on the trolley, one before and one after the transmission counters. These were used to measure continuously the efficiencies of the twelve transmission counters.

Three meters of iron shielding and two large scintillation counters, S_6 and S_7, were placed at the end of the beam. They were used in coincidence during the measurements of muon contamination.

Fig. 8 shows a schematic drawing of the target cells used in this experiment which were cylinders, 3 m long and 12 cm in diameter, containing hydrogen, deuterium and helium gas, at a pressure of ~ 70 atmospheres and at liquid-nitrogen temperature. The helium target was used in measurements of absorption cross-sections to be described later. This provided approximately 7 g/cm^2 of hydrogen and 14 g/cm^2 of deuterium and helium. The two end windows of the targets were constructed from stainless steel, each 1.3 mm thick. An identical evacuated dummy target was used for the empty target measurements. The gas pressure was monitored by precision manometers to an accuracy of ± 0.1 kg/cm^2 and the calibration of each instrument was carefully checked before and after each running period. The operating temperature of the gas was measured to an accuracy of ± 0.5°K by using the sealed cell as a gas thermometer in cooling it down from room temperature. The pressure and the temperature of the gas thus determined the hydrogen density by evaluation of the equation of state, as given by Rabinovich[6]. This method is in agreement within ± 0.2% with experimental data [7,8].

The estimated uncertainty of the hydrogen density is ± 0.7%. The deuterium density was calculated from the data of Michels et al.[8], which, however had to be extrapolated in temperature. This was done using the Beattie-Bridgeman equation of state[9], the constants of which were adapted to the existing data. Because of the extrapolation a larger error has been assigned to the deuterium density (± 0.9%). To check the reliability of the density calculations, the pion cross-sections were measured first with the targets filled to 70 atmospheres at room temperature, then after cooling to liquid-nitrogen temperature without adding gas

and finally at the operating pressure and liquid-nitrogen temperature. Some data were also taken using the CH_2-C difference technique.

The data were taken in four periods of accelerator operation. Each time, pion-cross-sections at 40 GeV/c were measured as a check on reproducibility. Measurements consisted of a series of runs where the particles transmitted through the target and detected by each transmission counter were recorded for a fixed number of monitor counts M. The series of runs was a cyclic permutation of measurements with the hydrogen, deuterium and dummy targets. At the end of each run, the data were transferred onto punched cards for off-line analysis, which was carried out on a MINSK 22 computer. Data were scrutinized to check that channel efficiencies were larger than ~ 99.5% and that the delayed coincidences in the largest transmission channel were smaller than 1.0% (2% for $\bar{p}$). The beam intensity was raised and lowered by a factor of three at 40 GeV/c and the resulting cross-sections were found to be in agreement within the statistical errors.

The extrapolation to zero solid angle was carried out using the relation

$$\sigma_i = \sigma_{tot} \exp \left(a t_i + b t_i^2\right) \qquad (1)$$

where σ_i is the partial cross-section measured by the i^{th} channel accepting a maximum four momentum squared t_i and σ_{tot} is the desired total cross-section. A typical example is shown in Fig. 9. This form gave statistically acceptable fits to the data in the t-range used, which was $0.014 < |t_i| < 0.065$ $(GeV/c)^2$. Thus usually the first two channels were ignored because of multiple scattering effects and the last channel used was T_8. The extrapolation t-range was varied by adding and subtracting one counter at the beginning and end of the range in order to check the stability of the extrapolated cross-section.

The spread in these five extrapolations was included when evaluating the final error quoted on a point. The parameter b in eq. (1) was poorly determined by the data for each point separately. So in the final fit it was kept fixed at the average value for the hydrogen and deuterium data, respectively. Extrapolations were also made without the quadratic term in the exponent of eq. (1) and also using a second-order polynomial expression in t_i. The fits obtained were statistically worse than those of eq. (1) and resulted in total cross-sections about 0.5% lower than quoted.

The pion cross-sections were corrected for muon contamination in the beam. The contamination was measured directly by utilizing the high resolution Čerenkov counter C and the coincidence signal S_6S_7 from the two counters behind the steel at the end of the beam. The correction arising from pion decay between C and the centre of the targets was computed and added to the measured contamination to yield a total μ correction of 2.5 ($\pm$ 0.5)% at 20 GeV/c, decreasing to 1.0 ($\pm$ 0.4)% at 65 GeV/c. As a check on this procedure, several cross-sections were remeasured with the signal S_6S_7 in anticoincidence with the transmission counters. The results were consistent with the data corrected as described. The kaon cross-sections have not been corrected for $K \to \mu$ decays, since this contamination produces a negligible effect on the extrapolated cross-sections. Other corrections (Coulomb, Coulomb-nuclear interference, and the effects of decays after the targets) are negligible at these energies in the t-range used.

From the total cross-sections on deuterium and hydrogen the total cross-sections on neutrons have been derived, using the Glauber formula[10] to take into account the shadow effect, neglecting the Fermi motion

$$\sigma_n = \sigma_d - \sigma_p + \delta \qquad (2)$$

where the shadow term δ is given by

$$\delta = \frac{\langle r^{-2} \rangle}{4\pi} \sigma_p \sigma_n . \qquad (3)$$

The real parts of the forward scattering amplitude have been neglected in eq. (3) since they are expected to be small. The more correct form of this equation due to Wilkin[11] gives the same results at these high energies where charge exchange scattering is negligible. $\langle r^{-2} \rangle$ is the mean inverse square separation between the proton and the neutron in the deuteron. For $\langle r^{-2} \rangle$, values as low as 0.02 mb^{-1} and as high as 0.042 mb^{-1} have been derived and used in the literature, but recently a convergence towards 0.030 mb^{-1} has developed. Such a value is in agreement with Hulthèn wave function calculations[10]. In the present work a value 0.030 mb^{-1} has therefore been adopted and, somewhat arbitrarily, an error of $\pm$ 0.005 mb^{-1} has been assigned to it.

Results are presented in table 1. The errors quoted are compounded of a purely statistical part, an extrapolation error, and point to point uncertainties on the muon correction. Not included is a scale error originating mainly from the uncertainties in the gas densities and in the correction for muon contamination. This error is listed at the foot of the table.

Fig. 10 shows the results of this experiment together with previous measurements[12-14]. In general the agreement of our lower energy data with earlier results is good, with the exception perhaps of the π^-p and π^-d cross-sections of Galbraith et al. The three graphs in the left column of Fig. 10 show the total cross-sections on hydrogen. Beyond 30 GeV/c the pion total cross-sections have become rather energy independent within the error of about $\pm$ 0.2 mb on each point, averaging about 24.6 $\pm$ 0.3 mb (this error includes the scale error). Similarly, the K^--p cross-section appears to be energy independent, averaging 20.9 $\pm$ 0.3 mb. Only the antiproton cross-section continues to decrease, reaching a value of about 44 mb at 50 GeV/c.

This value is ~10% to 15% larger than the estimated proton-proton total cross-section at this momentum. The behaviours of the p-p and K^+-p total cross-sections, as presently known, are shown by solid lines in the figure. It appears that both the K^--p and the K^+-p cross-sections have become constant but at quite different values.

The middle column shows the total cross-sections on deuterium. Qualitatively the behaviour is very similar to that of the hydrogen cross-sections.

In the last column the data on neutron cross-sections are shown. The π^--n and the K^--n cross-sections seem also to have approached energy-independent values, namely 23.3 ± 0.6 mb and 19.9 ± 0.5 mb, respectively. These values are close to the corresponding cross-sections on protons. The precise differences are $\sigma(\pi^-p) - \sigma(\pi^-n) = 1.3 \pm 0.7$ mb and $\sigma(K^-p) - \sigma(K^-n) = 1.0 \pm 0.6$ mb, the errors being partly due to the uncertainty in the hydrogen and deuterium density, partly due to the uncertainty in the Glauber correction.

The $\bar{p}$-n cross-sections are identical within errors to the corresponding $\bar{p}$-p data, over the whole range covered by this experiment. All these facts suggest that above 30 GeV/c the strong interaction cross-sections have become approximately independent of isospin, in accordance with the Okun'-Pomeranchuk rule[15].

If one makes the much weaker assumption of charge symmetry, the validity of which has been demonstrated at lower energies for instance by the accurate equality of π^--d and π^+-d total cross-sections, one can make the identification $\sigma(\pi^-n) = \sigma(\pi^+p)$. This enables a direct comparison to be made between the new data on π^--n and the precise π^+-p data at lower energies. This

has been done in the upper graph of the right hand column of fig. 10, where good agreement is seen in the region at 20 GeV/c.

There exists a wide range of theoretical predictions regarding the high-energy behaviour of total cross-sections, usually in the framework of Regge-pole theory. The more conventional models predict cross-sections that decrease towards a finite non-zero asymptotic limit. Other models predict vanishing total cross-sections at infinity. Still others predict total cross-sections rising logarithmically towards their asymptotic values. Fig. 11 shows the comparison of our data with the conventional Regge-pole fit of Barger et al.[16] to previously existing data. There is a difference between the apparent energy independence of the new π^- and K^- total cross-sections and the predictions of the model. The models that predict vanishing total cross-sections can probably be excluded already, since they predict an even steeper fall-off with energy. The data might be in agreement with a model predicting slowly rising cross-sections, although the present data do not establish such a trend.

According to the Pomeranchuk theorem[17], particle and antiparticle total cross-sections must become equal in the asymptotic region. For the pion nucleon system, where particle and antiparticle belong to the same isospin multiplet, the implications of the Okun'-Pomeranchuk rule are equivalent to those of the Pomeranchuk theorem. However, in the case of the strange mesons, there exists a significant difference of about 3 mb between the newly measured K^--p cross-sections and the extrapolated values of the previously measured K^+-p cross-sections, which already seemed to be energy independent below 20 GeV/c. If energy independence of total cross-sections is interpreted as indicating

the onset of the asymptotic region, then there exists a contradiction with the Pomeranchuk theorem. In order to avoid such a contradiction one must assume that in reality some weak energy dependence persists: either the K^--p cross-section has a very slow decrease with energy, not excluded by the present data, or the K^+-p cross-section must increase with energy, or both. In these cases the onset of the asymptotic region is still a long way off.

Before discussing further the implications of the new total cross-section results, and comparing various theoretical attempts to explain the effects observed, I would like to complete the presentation of the experimental results, with some data on absorption cross-sections for various nuclei.

Absorption Cross-Sections on Nuclei

The experimental technique used was essentially the same as for the total cross-section measurements, but using various nuclei as targets. The difference lies in the extrapolation procedure, where partial cross-sections measured by the larger counters T_9 to T_{12} were used, corresponding to $0.10 \leq |t_i| \leq 0.30$ GeV/c^2. Fits in this range were made using the formula :

$$\sigma_i = \sigma_{abs} \exp (at_i) \qquad (4)$$

Measurements of σ_{abs} were made on He, Li, Be, C, Al, Cu, Sn, Pb and U. An example of the data at 40 GeV/c for π^- is shown in Fig. 12. The H_2 and D_2 data are included for comparison. The steep rise of the partial cross-sections in the region $|t| \leq 0.05$ GeV/c^2 shown especially by the heavy nuclei is due to Coulomb and coherent diffraction scattering. It is because the latter is excluded from the extrapolation that one obtains σ_{abs} from these measurements.

The results obtained at various momenta and for various particles are shown in table 2. It is notable that there is very little energy dependence of σ_{abs} except for antiprotons between 20 and 30 GeV/c. Fig. 13 shows the dependence of σ_{abs} on atomic number for π^-, K^- and $\bar{p}$ at 40 GeV/c. The fitted straight lines are of the form :

$$\sigma = \sigma_o A^{\alpha} \qquad (5)$$

and α depends on the type of incident particle. The He data have not been included in the fit, because of larger uncertainty in the extrapolation procedure. Table 3 shows the results of the fit. Note that the antiproton data have a value of α close to 2/3, which is what one expects for a completely absorbing nucleus (black disc), while for π^-, and K^- the slopes are larger, indicating some degree of transparency.

Some data have also been taken on absorption cross-sections for $\bar{d}$ on Li, C, Al, Cu and Pb[1e]. Although statistically less significant than the $\bar{p}$ data, σ_{abs} for $\bar{d}$ also shows a value of α close to 2/3. The details of the work involving detection of $\bar{d}$ will be discussed by J.-P. Stroot in his contributed paper to this Conference.

Discussion of the Results

Comparison of the results of particle production measurements at different incident energies shows that to a first approximation the production cross-sections depend only on the elasticity and the transverse momentum of the produced particle. Liland and Pilkuhn[18] have formalized this experimental fact into a simple scaling law for meson production which can be represented as follows :

$$d^2\sigma(P_p, P, \Theta)/d\Omega\, dP = d^2\sigma(P_o, P', \Theta')/d\Omega'\, dP' \qquad (6)$$

where P_p is the incident proton momentum where predictions are required and P_o is the incident proton momentum where data exists. The secondary momenta and angles are related by :

$$P' = \left(P_o / P_p\right) . \ P \qquad : \qquad \Theta' = \left(P_p / P_o\right) \Theta \ .$$

Thus $d^2\sigma/d\Omega dP$ depends only on the meson elasticity P/P_p and the transferse momentum $P_T = P.\Theta$. This law should be valid for $P/P_p \gtrsim 0.5$.

Since the first presentation of the total cross-section results, many theoretical papers have appeared offering explanations for the "flattening" of the cross-sections and the apparent inequality of the K^+ and K^- cross-sections.

Barger and Phillips[19] make a successful fit to all the available data by adding cuts into a Regge model. Negative contributions from the leading vacuum cuts explain the levelling out of $\sigma_T(K^-N)$ and $\sigma_T(\pi^-N)$ above 25 GeV/c. Their fit is shown in Fig. 14. They also reconcile the apparently non-converging K^+N results with a common asymptotic limit, in accord with the Pomeranchuk theorem, but at levels considerably higher than the plateaus reached by the data at present energies. The exact values of σ_T^∞ are dependent on secondary pole effects and are not firm predictions but are shown in Fig. 15. The striking fact is that if "asymptopia" is defined as the region beyond which σ_T differs by less than ± 0.2 mb it will not be reached until 10^{98} GeV/c for πN and 10^{53} GeV/c for KN scattering, in the framework of their fit.

Tomozawa[20] has considered the possibility that the Pomeranchuk theorem may be violated from purely theoretical considerations based on the quark model, even before the results of this experiment were released. Other authors, including Martin[21], Eden[22], and Horn[23] question the validity of the Pomeranchuk theorem, on the basis of the IHEP-CERN results, and emphasize that one can obtain unequal particle - antiparticle asymptotic cross-sections if the real

part of the scattering amplitude dominates at high energies. Horn suggests a novel mechanism for this starting from the data plotted in the form shown in Fig. 16. Noting the sharp "break" in the region of 30 GeV/c and wishing to keep the simple behaviour exhibited by the data below 30 GeV/c he argues that either $\sigma_T \propto S^{-1/2}$ or it is constant. As a physical argument for this discontinuous behaviour he conjectures that the break occurs as a reflection of an "ionisation point" - the energy at which resonances cease to exist. This might be understood in a naive quark model, in which resonances are bound states of quarks, the ionization point corresponding to the sum of the masses of three such quarks.

The Second IHEP - CERN Experiment

The next experiment to be carried out by a joint IHEP-CERN team will be a search for new boson resonances, X^- in the mass range $4 < M_X < 8$ GeV. The liquid hydrogen target and the whole detection equipment have all been tested in CERN and on April 1st will all be flown to Moscow in a giant Antonov cargo airplane of the Soviet Airline "Aeroflot".

The experiment is based on the techniques used for many years by the CERN boson spectrometer group. The measurement of the momentum and angle of the slow forward going proton produced in the reaction :

$$\pi^- + p \rightarrow p + X^-$$

by a large aperture magnet and wire spark chambers enables the "missing mass" of the X^- to be precisely evaluated. The direction of the decay products of the X^- are measured by wide gap spark chambers with magnetostrictive read-out. The data acquisition system contains 250 scalers on-line to an IBM 1800 computer.

Initially the experiment will be installed in channel 4B and will cover the mass range up to 6.6 GeV with π^- beams up to 40 GeV/c. Later it will move to channel 2 to cover the higher mass and momentum range.

Conclusions

The important conclusion to be drawn from the results of the first phase of this experiment is that refined application of well established Čerenkov techniques is adequate for particle identification in this momentum range. Thus one has reason to believe that even for beams from the future accelerators in the 200-300 GeV range, Čerenkov techniques will play a major role in particle identification. Furthermore, using the data obtained at the IHEP accelerator one can make reasonable estimates of the beam intensities which will become available in the future.

The total cross-section data from the CERN - IHEP experiment have caused us to drastically rethink our ideas of "asymptopia". It is clear that more data on total cross-sections, especially for positive particles, are needed in the high energy region. Such measurements could presumably decide whether we have cuts or whether the Pomeranchuk theorem fails. In addition the phase of the scattering amplitude in the forward direction could be a vital clue to the mechanisms at work. Measurements of Coulomb-Nuclear interference for p-p scattering and of K°-regeneration, at present in progress at the IHEP accelerator should be very revealing from this aspect.

If the real parts of the scattering amplitude do start to dominate, because of a logarithmic rise with energy, as is predicted if the Pomeranchuk theorem is violated, then $(d\sigma/dt)_{t=o}$ will grow faster than σ_T by a factor $\log^2 s$.

Since $\sigma_{el} < \sigma_T$, we should observe a shrinking forward peak at very high energies. This might be amenable to measurement at the 200 GeV accelerator, and certainly should be visible at the ISR in CERN but limited of course to p-p scattering where shrinking of the forward peak has already been seen up to 70 GeV by the Dubna group working at the IHEP machine.

The study and search for high energy bosons in the second IHEP - CERN experiment should reveal whether other drastic revisions in our ideas are necessary. Do we have a continuing family of bosons up to higher and higher energies, or will there be an "ionisation point"as suggested by Horn ?

Whatever answers are given in the next two years, I am sure there will be even more questions posed and that the 200 GeV accelerator will have some very exciting physics to discover.

Table 1

Results of the total cross-section measurements. The point to point errors are given in the table, the additional scale errors are given at the bottom of the table.

Laboratory Momentum [GeV/c]	Total cross-sections [mb]								
	$\pi^- p$	$K^- p$	$\bar{p}p$	$\pi^- d$	$K^- d$	$\bar{p}d$	$\pi^- n$	$K^- n$	$\bar{p}n$
20	25.38 ± 0.30	21.2 ± 0.6	49.0 ± 1.1	47.28 ± 0.60	39.3 ± 0.6	89.5 ± 1.3	23.3 ± 0.6	19.1 ± 0.8	46.0 ± 1.7
25	24.85 ± 0.25	20.7 ± 0.4	46.1 ± 0.6	47.14 ± 0.50	39.4 ± 0.5	86.5 ± 0.9	23.7 ± 0.5	19.7 ± 0.6	45.3 ± 1.1
30	24.97 ± 0.15	21.3 ± 0.3	47.1 ± 0.6	47.17 ± 0.30	40.4 ± 0.4	87.0 ± 0.9	23.6 ± 0.3	20.1 ± 0.5	44.9 ± 1.1
35	24.75 ± 0.15	20.8 ± 0.3	45.5 ± 0.7	46.85 ± 0.30	39.8 ± 0.4	86.4 ± 1.0	23.5 ± 0.3	19.9 ± 0.5	45.9 ± 1.2
40	24.70 ± 0.15	20.9 ± 0.3	45.0 ± 0.7	46.40 ± 0.30	39.3 ± 0.4	83.5 ± 0.9	23.1 ± 0.3	19.4 ± 0.5	43.2 ± 1.1
45	24.27 ± 0.15	20.6 ± 0.3	44.9 ± 0.7	46.20 ± 0.30	39.9 ± 0.4	84.8 ± 0.9	23.3 ± 0.3	20.2 ± 0.5	44.6 ± 1.1
50	24.62 ± 0.15	21.0 ± 0.4	43.6 ± 0.8	46.63 ± 0.30	39.9 ± 0.5	83.1 ± 0.9	23.4 ± 0.3	19.9 ± 0.6	44.1 ± 1.2
55	24.64 ± 0.15	21.5 ± 0.6		46.44 ± 0.30	40.9 ± 0.8		23.2 ± 0.3	20.4 ± 1.0	
60	24.60 ± 0.15			46.62 ± 0.30			23.4 ± 0.3		
65	24.69 ± 0.20			46.76 ± 0.30			23.4 ± 0.3		
Adtl.scale error	± 1%	± 1%	± 1%	± 1.2%	± 1.2%	± 1.2%	± 2.5%	± 2.5%	± 3%

TABLE 2

Absorption cross-sections in mb per nucleus.

Mom. (GeV/c)	Part.	Nucleus and atomic numbers. He 4.0	Li 6.94	Be 9.01	C 12.01	Al 26.98	Cu 63.54	Su 118.7	Pb 207.2	U 238
20	π^-	-	126 ± 2	154 ± 2	186 ± 3	349 ±7	657 ± 10	1044 ± 12	1550 ± 20	1860 ± 70
	K^-	-	110 ± 3	144 ± 5	169 ± 4	310 ±10	555 ± 20	885 ± 50	1330 ± 70	1600 ± 200
	$\bar{p}$	-	215 ± 7	240 ± 10	290 ± 15	500 ±20	965 ± 60	1300 ± 120	1810 ±150	2030 ± 320
30	π^-	73 ±3	120 ± 2	149 ± 3	177 ±2	340 ± 6	640 ± 8	1030 ± 20	1525 ± 25	1815 ± 35
	K^-	65 ±3	107 ± 2	134 ± 4	157 ± 3	308 ±10	616 ± 22	933 ± 20	1385 ± 45	1615 ± 80
	$\bar{p}$	117 ±5	188 ± 4	235 ± 6	258 ± 6	457 ±11	890 ± 30	1210 ± 45	1880 ± 65	2020 ± 125
40	π^-	74 ±3	121 ± 2	148 ± 2	179 ± 2	339 ±4	640 ± 7	1040 ± 15	1510 ± 20	1710 ± 35
	K^-	65 ±3	105 ± 2	137 ± 2	162 ± 2	313 ±6	593 ± 10	920 ± 30	1408 ± 30	1600 ± 50
	$\bar{p}$	119 ±5	168 ± 8	226 ± 7	257 ± 5	490 ±15	820 ± 30	1240 ± 70	1790 + 80	1820 ± 200
50	π^-	76 ±3	124 ± 2	149 ± 2	178 ± 2	338 ±4	635 ± 7	1040 ± 15	1525 ± 20	1700 ± 25
60	π^-	74 ±3	123 + 3	151 + 3	182 ± 3	340 ±4	654 ± 15	1020 ± 20	1510 ± 25	1775 ± 50

TABLE 3

Results of the least square fits of the absorption cross-sections to the formula $\sigma_{abs} = \sigma_o A^{\alpha}$. All the nuclei except He have been fitted, giving 8 data points.

Part.	Mom. (GeV/c)	α	σ_o (mb)	χ^2
π^-	20	0.743 ± 0.003	30.0 ± 0.5	6.2
	30	0.760 ± 0.005	27.4 ± 0.7	13.4
	40	0.750 ± 0.004	28.2 ± 0.5	9.8
	50	0.748 ± 0.004	28.5 ± 0.6	12.2
	60	0.745 ± 0.004	29.1 ± 0.6	5.8
K^-	20	0.727 ± 0.007	27.7 ± 0.9	4.4
	30	0.765 ± 0.007	24.3 ± 0.7	8.3
	40	0.759 ± 0.006	25.0 ± 0.7	14.3
$\bar{p}$	20	0.648 ± 0.010	59.1 ± 2.6	4.2
	30	0.674 ± 0.009	50.9 ± 2.4	15.2
	40	0.674 ± 0.010	49.9 ± 2.4	9.5

REFERENCES

(1) a. Yu.B. Bushnin, S.P. Denisov, S.V. Donskov, A.F. Dunaitsev, Y.P. Gorin, V.A. Kachanov, Yu.S. Khodirev, V.I. Kotov, V.M. Kutyin, A.I. Petrukhin, Yu.D. Prokoshkin, E.A. Razuvaev, R.S. Shuvalov, D.A. Stoyanova, and J.V. Allaby, F. Binon, A.N. Diddens, P. Duteil, G. Giacomelli, R. Meunier, J.-P. Peigneux, K. Schlüpmann, M. Spighel, C.A. Stahlbrandt, J.-P. Stroot and A.M. Wetherell,
Physics Lett. 29B, 48 (1969) and Yadernaya Fisika 10, 585 (1969).

b. F. Binon, S.P. Denisov, P. Duteil, V.A. Kachanov, V.M. Kutyin, J.-P. Peigneux, Yu.D. Prokoshkin, E.A. Razuvaev, R.S. Shuvalov, M. Spighel and J.-P. Stroot,
Physics Lett. 30B, 506 (1969).

c. J.V. Allaby, Yu.B. Bushnin, S.P. Denisov, A.N. Diddens, R.W. Dobinson, S.V. Donskov, G. Giacomelli, Y.P. Gorin, A. Klovning, A.I. Petrukhin, Yu.D. Prokoshkin, R.S. Shuvalov, C.A. Stahlbrandt, and D.A. Stoyanova,
Physics Lett. 30B, 500 (1969).

d. F. Binon, P. Duteil, V.A. Kachanov, V.P. Khromov, V.M. Kutyin, V.G. Lapshin, J.-P. Peigneux, Yu.D. Prokoshkin, E.A. Razuvaev, V.I. Rykalin, R.S. Shuvalov, V.I. Solianik, M. Spighel, J.-P. Stroot and N.K. Vish evsky,
Phys.Lett. 30B, 510 (1969).

e. F. Binon, S.P. Denisov, S.V. Donskov, P. Duteil, G. Giacomelli, Yu.P. Gorin, V.A. Kachanov, V.M. Kutyin, J.-P. Peigneux, A.I. Petrukhin, Yu.D. Prokoshkin, E.A. Razuvaev, R.S. Shuvalov, D.A. Stoyanova, J.-P. Stroot,
Phys.Lett. 31B, 230 (1970).

(2) P. Duteil, L. Gilly, R. Meunier, J.-P. Stroot and M. Spighel,
Rev.Sc.Instrum. 35 (1964) 1523.

(3) Yu.D. Prokoshkin, IHEP preprint 69-7 (1969).

(4) J.B. Cumming, Am.Rev.Nucl.Science 13 (1963) 261.

(5) J.V. Allaby, F. Binon, A.N. Diddens, P. Duteil, A. Klovning, R. Meunier, J.P. Peigneux, E.J. Sacharidis, K. Schlüpmann, M. Spighel, J.-P. Stroot, A.M. Thorndike and A.M. Wetherell,
submitted to the 14th Internat. Conference on High Energy Physics, Vienna (1968) (CERN, Geneva, 1968).

(6) W.A. Rabinovich, Inzh.-Fiz. Zhur., Akad. Nauk Belorussk. SSR 5, 30 (1962).

(7) J. Hilsenrath, C.W. Beckett, W.S. Benedict, L. Fano, H.J. Hoge, J.F. Masi, R.L. Nuttall, Y.S. Touloukiar and H.W. Woolley,
"Tables of Termal Properties of Gases", National Bureau of Standards (Washington), Circular 564 (1955).

R.D. Goodwin, D.E. Diller, H.M. Roder and L.A. Weber,
Journal of Research NBS 68A, 121 (1964).

H.L. Johnston and D. White,
Trans.Am.Soc.Mech.Eng. 72, 785 (1950).

(8) A. Michels, W. de Graaff, T. Wassenaar, J.M.H. Levelt, and P. Louwerse,
Physica 25, 25 (1959).

(9) J.A. Beattie and W.H. Stockmayer,
Rep.Progr.Physics 7, 195 (1940).

(10) R.J. Glauber, Phys.Rev. 100, 242 (1955).
V. Franco and R.J. Glauber, Phys.Rev. 142, 1195 (1966).

(11) C. Wilkin, Phys.Rev. Letters 17, 561 (1966).

(12) W. Galbraith, E.W. Jenkins, T.F. Kycia, B.A. Leontic, R.H. Phillips, A.L. Read, and R. Rubinstein,
Phys.Rev. 138B, 913 (1965).

(13) G. von Dardel, D. Dekkers, R. Mermod, M. Vivargent, G. Weber, and K. Winter, Phys.Rev. Letters 8, 173 (1962).

(14) K.J. Foley, R.S. Jones, S.J. Lindenbaum, W.A. Love, S. Ozaki, E.D. Platner, C.A. Quarles, E.H. Willen,
Phys.Rev.Letters 19, 330, 857 (1967).

(15) L.B. Okun' and I.Ia. Pomeranchuk, Zhur. Eksp. i Teoret.Fiz. 30, 424 (1956) (English Translation: Soviet Phys. - JETP 3, 307 (1956)).

(16) V. Barger, M. Olsson and D.D. Reeder, Nuclear Physics B5, 411 (1968).

(17) I.Ia. Pomeranchuk, Zhur.Eksp. i Teoret. Fiz. 34, 725 (1958) (English Translation: Soviet Phys. - JETP 7, 499 (1958).).

(18) A. Liland and H. Pilkuhn, Phys.Lett. 29B, 663 (1969).

(19) V. Barger and R.J.N. Phillips, Phys.Rev.Lett. 24, 291 (1970).

(20) Y. Tomozawa, Phys.Rev. 186, 1504 (1969).

(21) A. Martin, CERN preprint TH 1075, Sept. 1969.

(22) R.J. Eden, UCR - 34P107 - 105, Submitted to Phys.Rev.Lett.

(23) D. Horn, Phys.Lett. 31B, 30 (1970).

Figure Captions

Fig. 1 : Layout of the experimental area at the IHEP 70 GeV accelerator.

Fig. 2 : Layout of the beam. 1, 2, 3 indicate the positions of the internal aluminium targets. K_1, K_2, and K_3 are collimators; L_1 - L_{10} are quadrupole lenses, M_1 - M_3 bending magnets. D, Δ indicate differential Čerenkov counters, C_1 - C_3 threshold Čerenkov counters. The scintillation counters A_1 - A_3 were used in conjunction with D, S_1 - S_5 in conjunction with Δ and C_1 - C_3. Scintillation counters S_6, placed after the iron absorber, was used to measure the muon contamination of the beam. P_{123} and F_{1234} are monitor telescopes.

Fig. 3 : Pressure curves at different momenta obtained with a) the D counter, b) the Δ counter, c) the threshold counter combination $\bar{C}_1\, C_2\, \bar{C}_3$, and d) the differential-threshold combination $C_1 * C_2 * \bar{C}_3$.

Fig. 4 : Antideuteron identification with the differential Čerenkov counter. N is the number of interference fringes (the refraction index of the gas is measured with an interferometer). $p = 25.1$ GeV/c, $\Theta = 12$ mrad.

Fig. 5 : Laboratory spectra for π^-, K^-, $\bar{p}$ and $\bar{d}$ produced in 70 GeV/c proton aluminium interactions. The left-hand scale gives the double differential cross-section per aluminium nucleus; the right-hand scale gives the flux per 10^{12} circulating protons into a momentum band of $\Delta P = 1$ GeV/c and a collimator 4 x 4 cm (solid angle $\Delta\Omega = 8 \times 10^{-6}$ sr). The lines are interpolated values for the spectra at 0 mrad. The solid points are for Θ 5 mrad, the open points are in the range $5 < \Theta < 15$ mrad. The exact production angles are given in Reference 1.

Fig. 6 : Particle ratios versus beam laboratory momentum divided by the kinematically allowed maximum momentum of the heavier particle (K^- and $\bar{p}$, respectively). The broken line represents the 19.2 GeV/c CERN data for p-p collisions, and coincides with the dependence found by the same group for p-Al collisions (unpublished).

Fig. 7 : Layout of the beam and of the experimental equipment. 1, 2, and 3 indicate the positions of the internal aluminium targets. K_1, K_2, and K_3 are collimators, L_1 - L_{10} are quadrupole lenses, M_1 - M_4 are bending magnets, S_1 - S_7 are scintillation counters, A_1 and A_2 are anti-coincidence scintillation counters, D and Č are the differential and the threshold Čerenkov counters, T_1 - T_{12} are the transmission counters; H_2, D_2, He and E are the target cells. F_{1-4} and P_{1-3} are monitor telescopes. G_2 are the nuclear targets.

Fig. 8 : Schematic diagram of a gas target.

Fig. 9 : Example of the extrapolation procedure to zero solid angle for π^-P and π^-D total cross-section measurements at 40 GeV/c. The fit shown by solid line is the one finally adopted.

Fig. 10: Total cross-section on hydrogen (left column), deuterium (middle column), and neutrons (right column) for π^- (top row), K^- (middle row), and $\bar{p}$ (bottom row) particles. The scale errors are not shown (see Table). The value $\langle r^{-2} \rangle = 0.03$ has been used in the Glauber-Wilkin correction. Some hand fits to positive particle total cross-sections are shown for comparison (full line). △: See ref. 12; +: See ref. 13; O : See Ref. 14 ●: this experiment.

Fig. 11: Comparison of the negative particle total cross-sections with the Regge-pole model predictions of Barger, Olsson and Reeder (ref. 16). The scale errors are not shown (see Table).

Fig. 12 : The extrapolation of the partial cross-sections to zero solid angle for 40 GeV/c π^- on nuclei to obtain the absorption cross-section. For reasons of completeness also the H_2 and D_2 partial cross-sections are shown.

Fig. 13 : Absorption cross-sections for 40 GeV/c π^-, K^- and $\bar{p}$ as function of A. The lines are fits to eq. (5).

Fig. 14 : Regge model fit of Barger and Phillips[19].

Fig. 15 : Projection of the total cross-sections to ultra-high energies, using the Barger-Phillips fit.

Fig. 16 : Total cross-sections for $\pi^{\pm}p$ plotted against $E^{-1/2}$, where E is the laboratory energy of the incident pion.

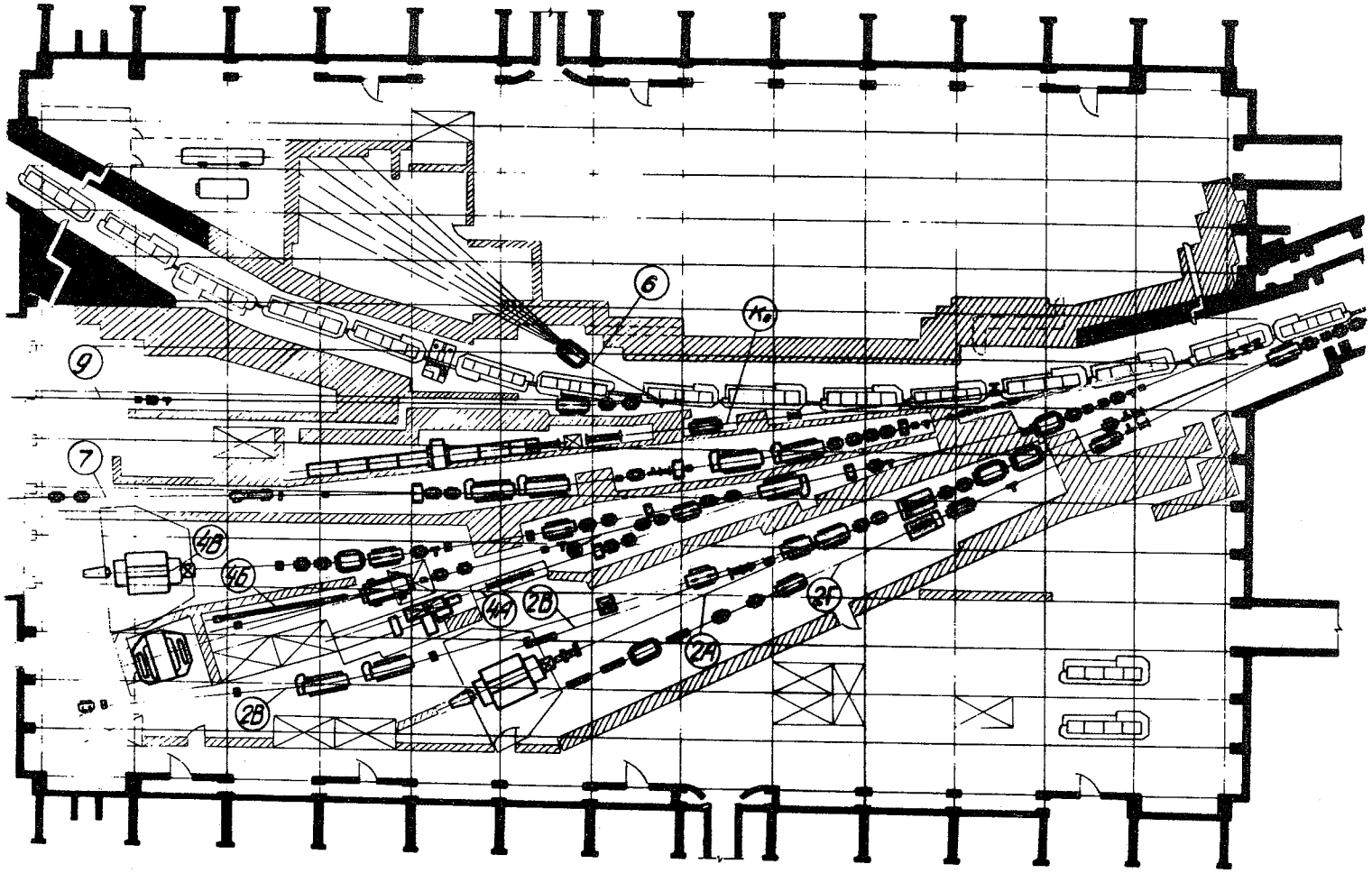

Fig:1

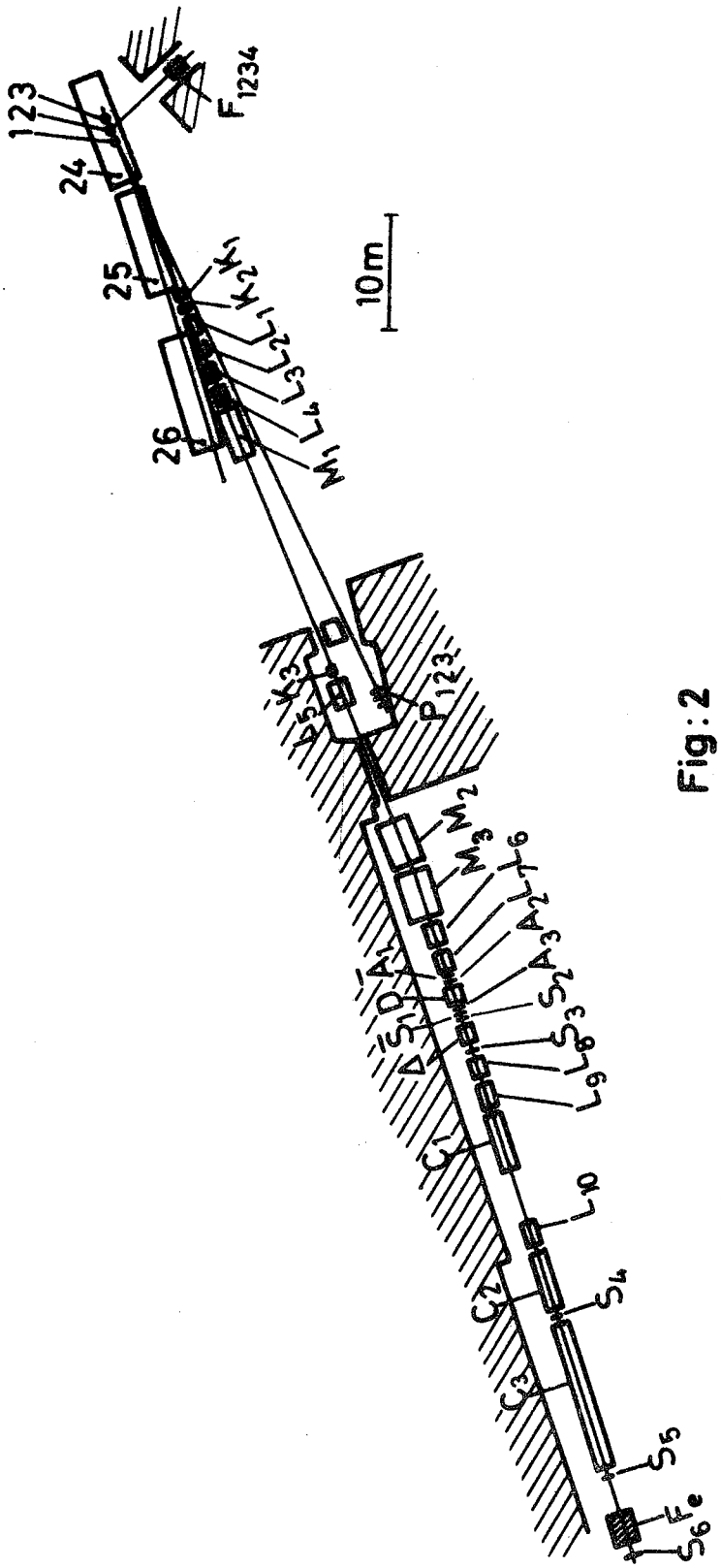
123
24
25
26
F_{1234}
10m
K_1
K_2
L_1
L_2
L_3
L_4
M_1
K_3
A_5
P_{123}
M_2
M_3
L_6
A_2
S_2
A_3
L_8
S_3
L_9
A_1
S_1
C_1
L_{10}
C_2
S_4
C_3
S_5
S_6

Fig:2

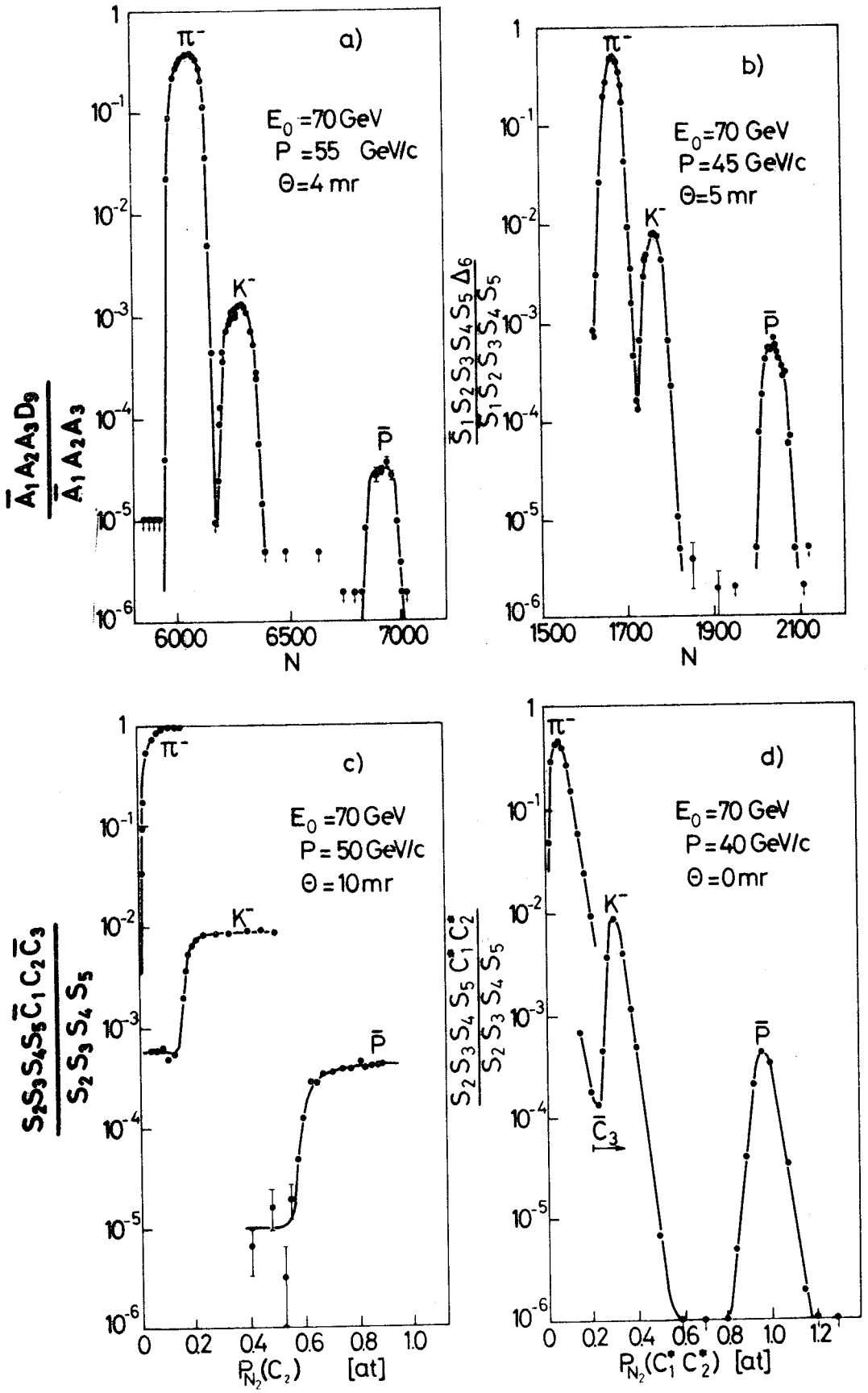
a)
E_0 =70 GeV
P =55 GeV/c
Θ=4 mr
π^-
K^-
$\bar{p}$
$\frac{\bar{A}_1 A_2 A_3 D_9}{\bar{A}_1 A_2 A_3}$
N
b)
E_0=70 GeV
P=45 GeV/c
Θ=5 mr
$\frac{\bar{S}_1 S_2 S_3 S_4 S_5 \Delta_6}{S_1 S_2 S_3 S_4 S_5}$
c)
E_0 =70 GeV
P = 50 GeV/c
Θ = 10mr
$\frac{S_2 S_3 S_4 S_5 \bar{C}_1 C_2 \bar{C}_3}{S_2 S_3 S_4 S_5}$
$P_{N_2}(C_2)$ [at]
d)
E_0 =70 GeV
P=40 GeV/c
Θ=0mr
$\bar{C}_3$
$\frac{S_2 S_3 S_4 S_5 C_1^* C_2^*}{S_2 S_3 S_4 S_5}$
$P_{N_2}(C_1^* C_2^*)$ [at]

Fig: 3

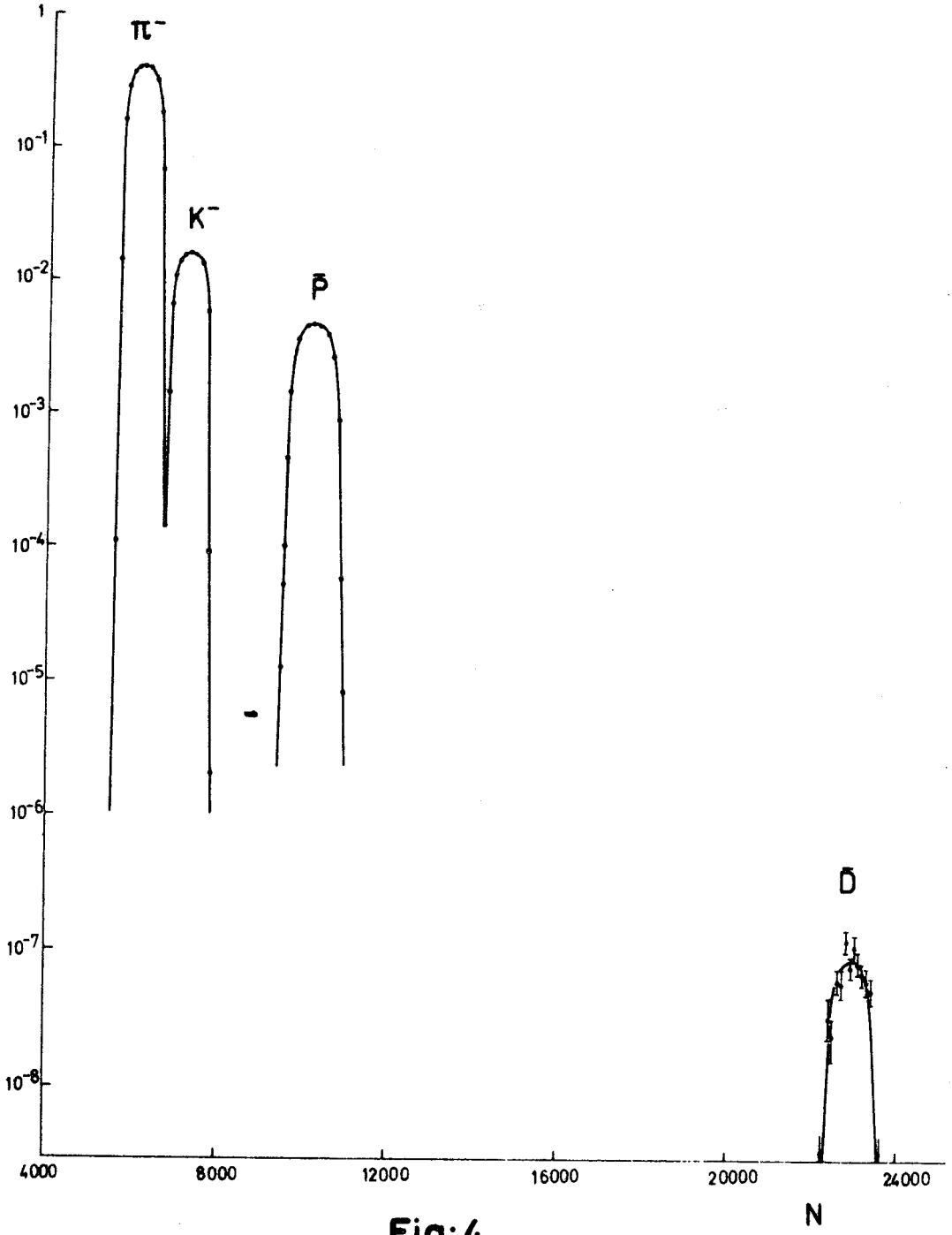
1
10^{-1}
10^{-2}
10^{-3}
10^{-4}
10^{-5}
10^{-6}
10^{-7}
10^{-8}
π^-
K^-
$\bar{p}$
$\bar{D}$
4000
8000
12000
16000
20000
24000
N

Fig:4

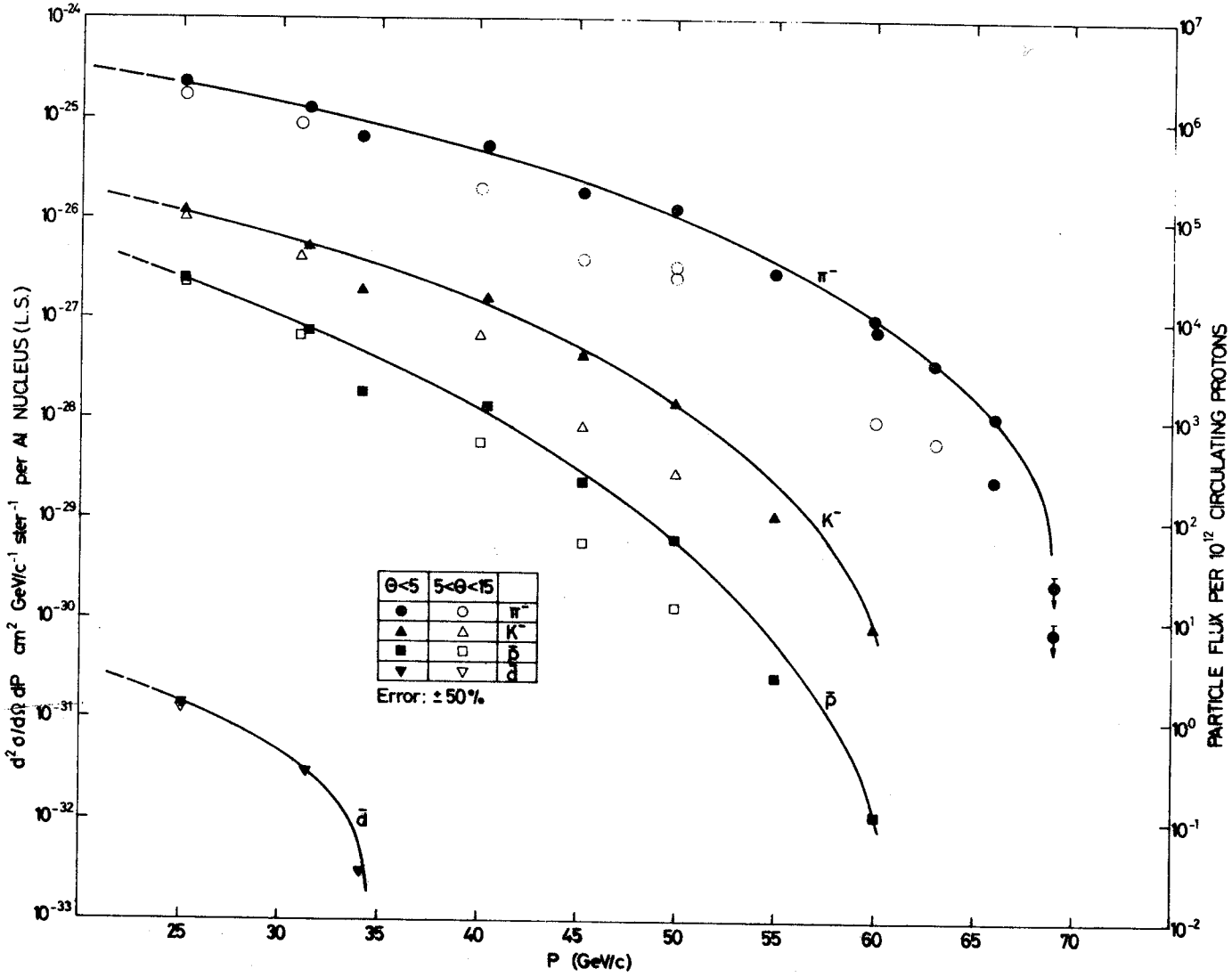
$d^2\sigma/d\Omega\,dP$ cm^2 GeV/c^{-1} ster^{-1} per Al NUCLEUS (L.S.)
PARTICLE FLUX PER 10^{12} CIRCULATING PROTONS
P (GeV/c)
π^-
K^-
$\bar{p}$
$\bar{d}$
θ<5 | 5<θ<15
Error: ± 50%

Fig:5

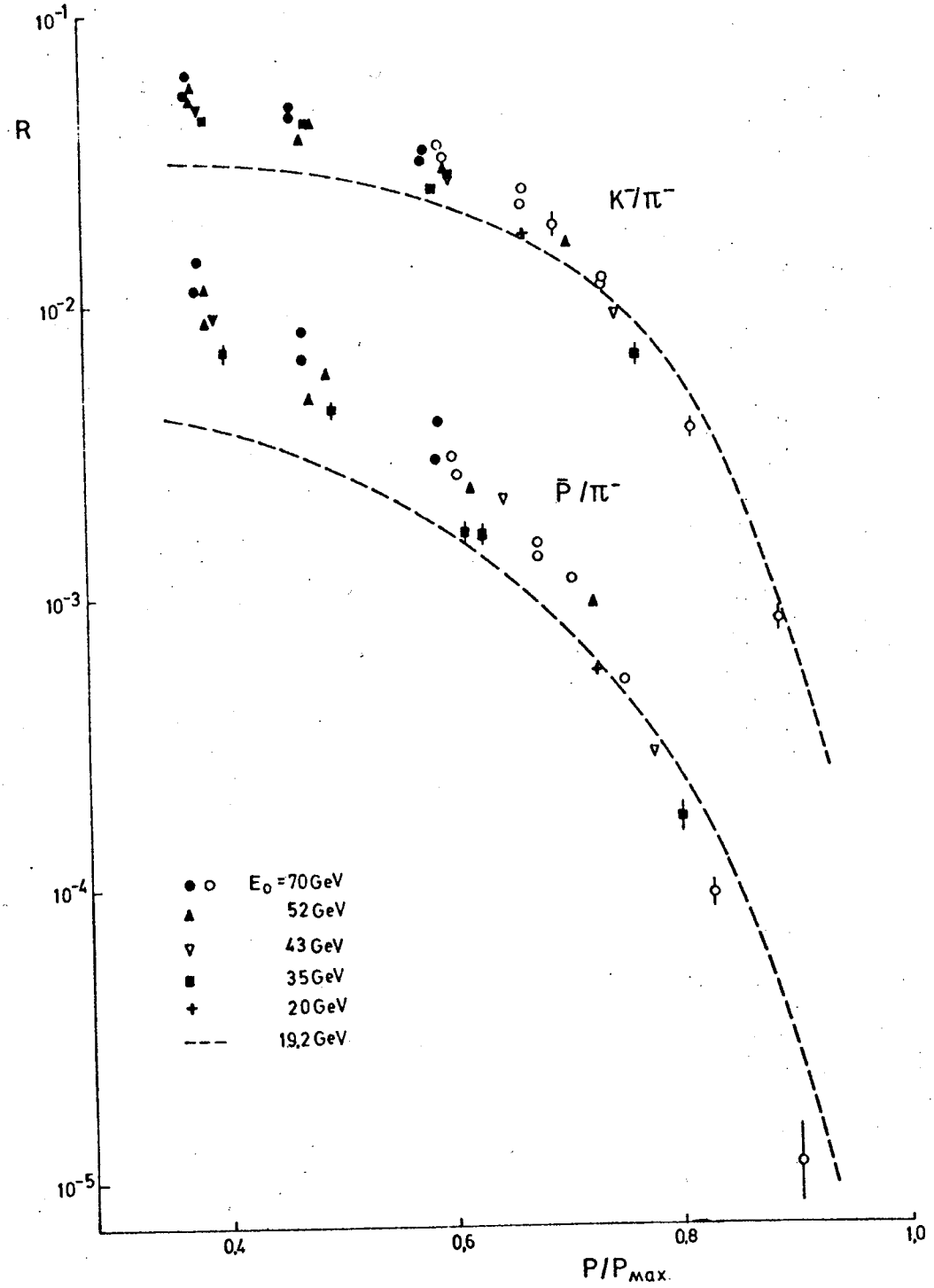
R
10^{-1}
10^{-2}
10^{-3}
10^{-4}
10^{-5}
K^-/π^-
$\bar{P}/\pi^-$
E_0 = 70 GeV
52 GeV
43 GeV
35 GeV
20 GeV
19,2 GeV
0,4
0,6
0,8
1,0
P/P_{max}

Fig:6

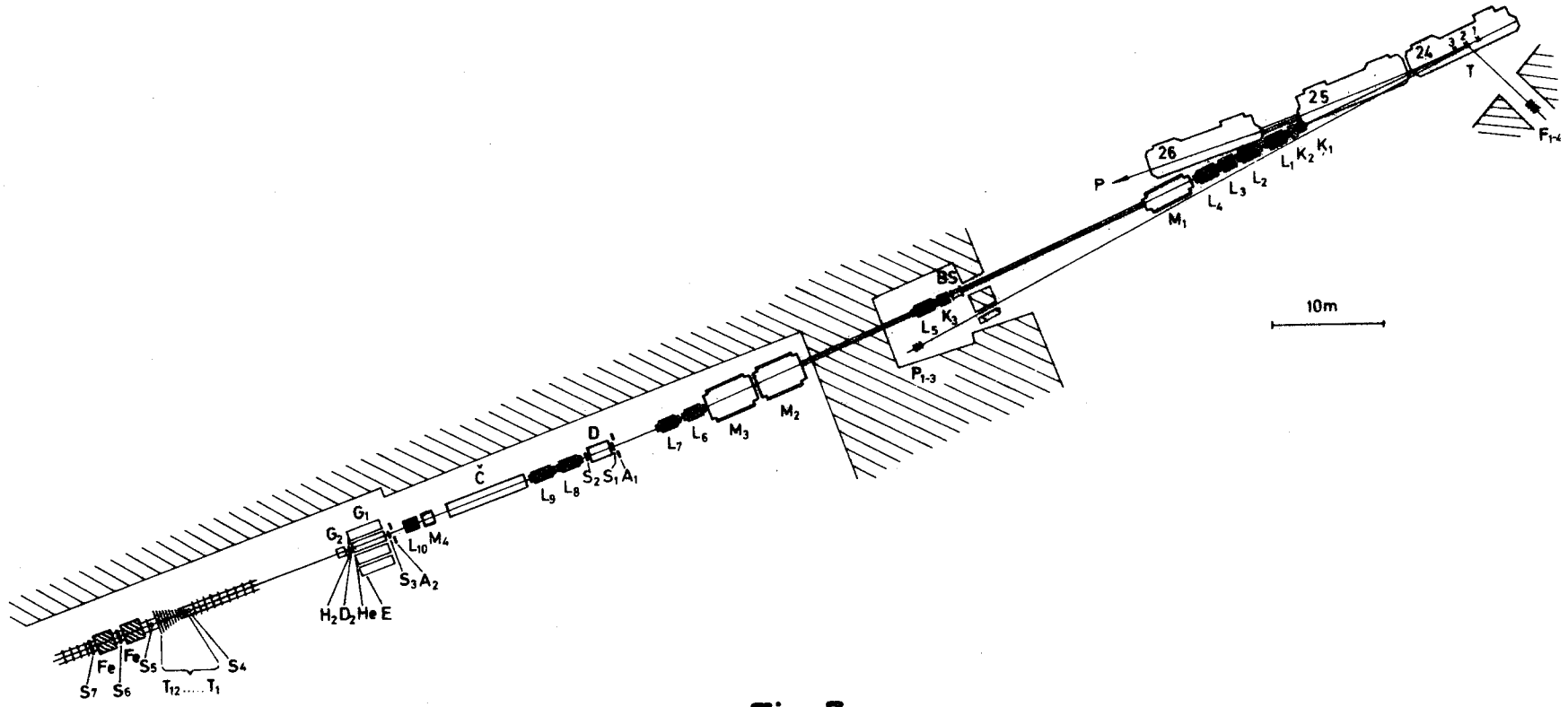
24
25
26
T
F1-4
P
M1
L4
L3
L2
L1
K2
K1
BS
L5
K3
P1-3
10m
M2
L7
L6
M3
D
S2
S1
A1
Č
L9
L8
G1
G2
L10
M4
S3
A2
H2
D2
He
E
Fe
Fe
S7
S6
S5
T12
T1
S4

Fig:7

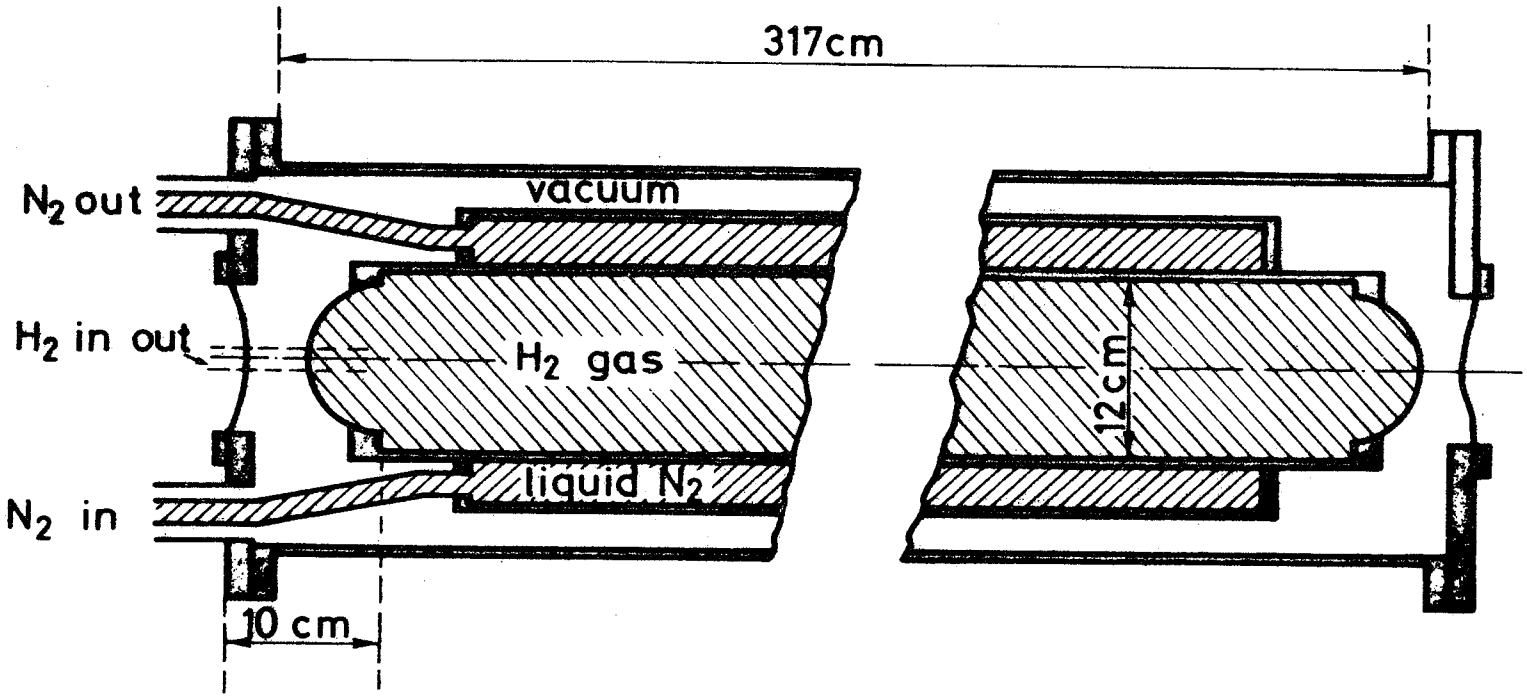

SCHEMATIC OF A GAS TARGET GEOMETRY

Fig: 8

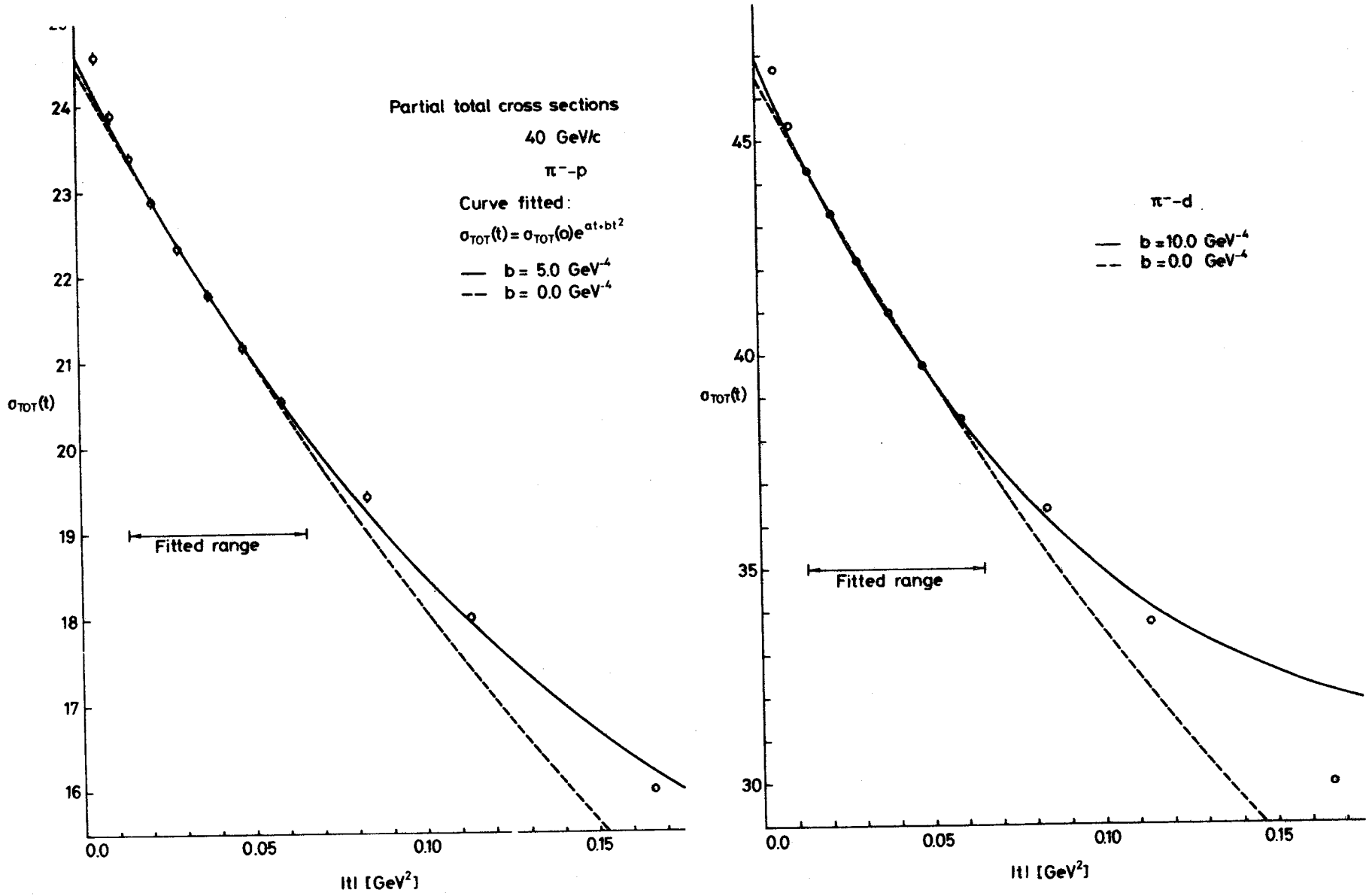
Partial total cross sections
40 GeV/c
π⁻-p
Curve fitted:
$\sigma_{TOT}(t) = \sigma_{TOT}(o)e^{at+bt^2}$
— b = 5.0 GeV⁻⁴
-- b = 0.0 GeV⁻⁴
Fitted range
$\sigma_{TOT}(t)$
|t| [GeV²]
π⁻-d
— b =10.0 GeV⁻⁴
-- b =0.0 GeV⁻⁴
Fitted range
$\sigma_{TOT}(t)$
|t| [GeV²]

Fig:9

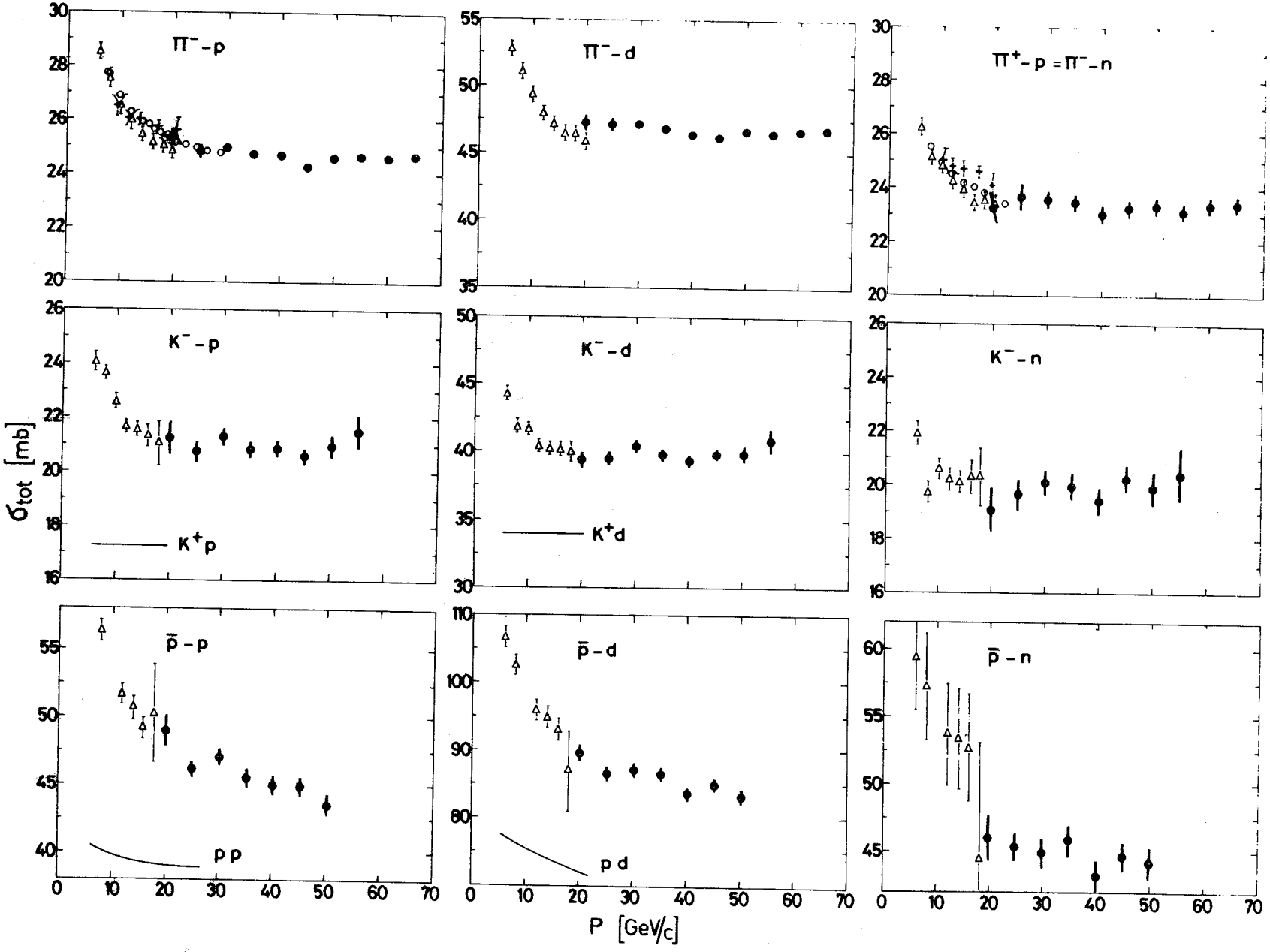

Fig:10

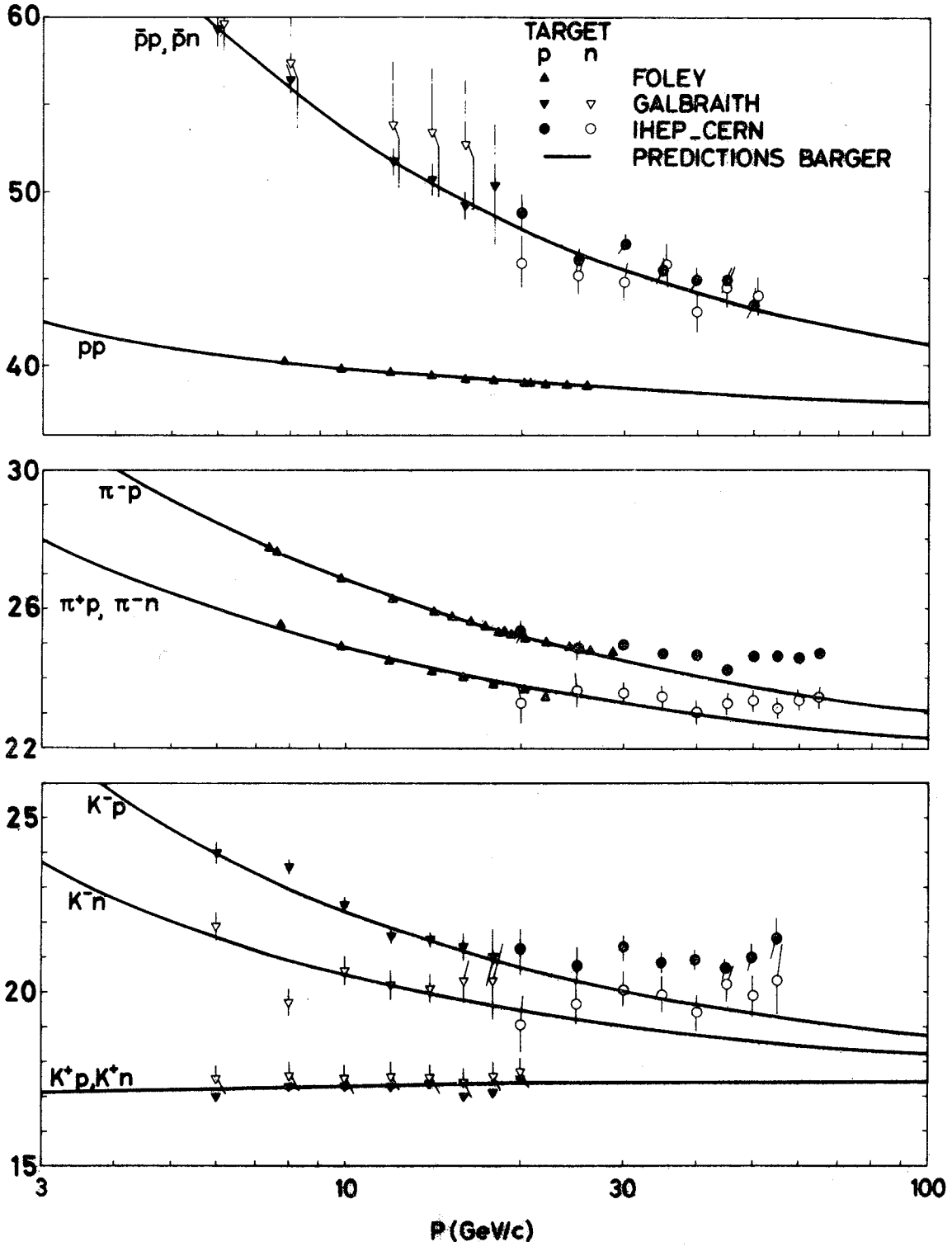
60
50
40
30
26
22
25
20
15
3
10
30
100
P(GeV/c)
$\bar{p}p, \bar{p}n$
pp
$\pi^- p$
$\pi^+ p, \pi^- n$
$K^- p$
$K^- n$
$K^+ p, K^+ n$
TARGET
p n
FOLEY
GALBRAITH
IHEP_CERN
PREDICTIONS BARGER

Fig : 11

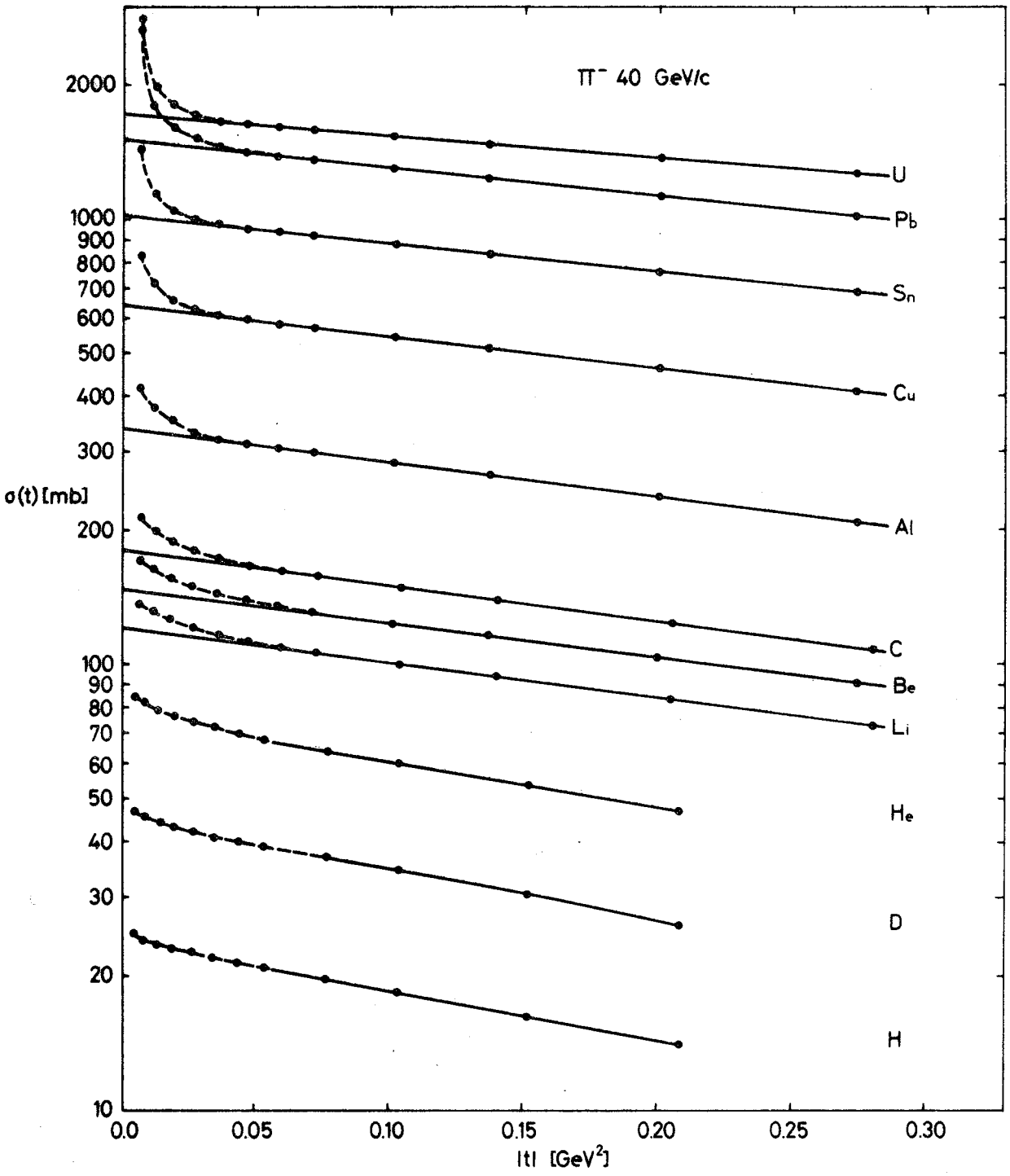
π⁻ 40 GeV/c
U
Pb
Sn
Cu
Al
C
Be
Li
He
D
H
σ(t) [mb]
2000
1000
900
800
700
600
500
400
300
200
100
90
80
70
60
50
40
30
20
10
0.0
0.05
0.10
0.15
0.20
0.25
0.30
|t| [GeV²]

Fig: 12

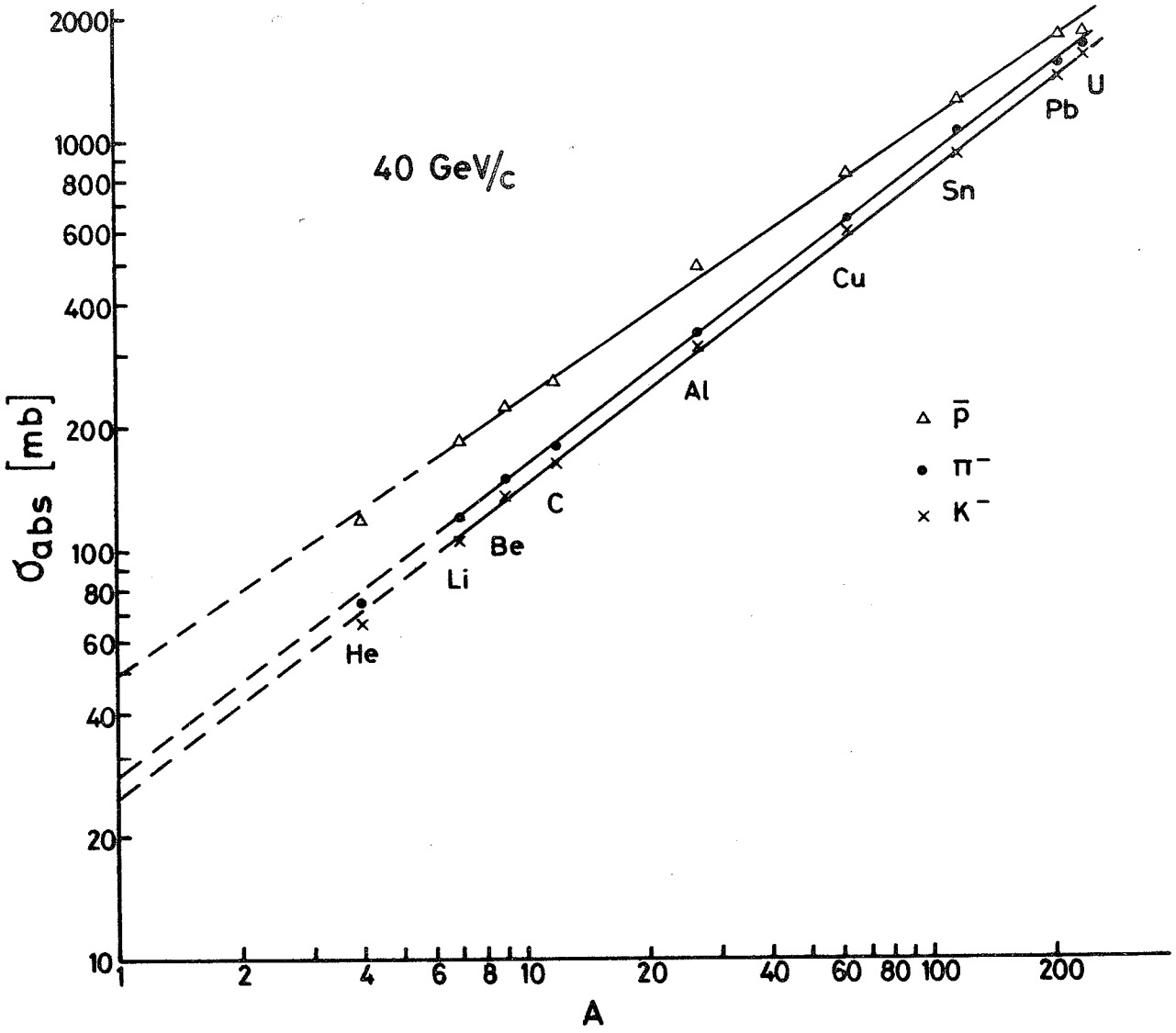
40 GeV/c
σ_{abs} [mb]
A
2000
1000
800
600
400
200
100
80
60
40
20
10
1
2
4
6
8
10
20
40
60
80
100
200
He
Li
Be
C
Al
Cu
Sn
Pb
U
$\bar{p}$
π^-
K^-

Fig:13

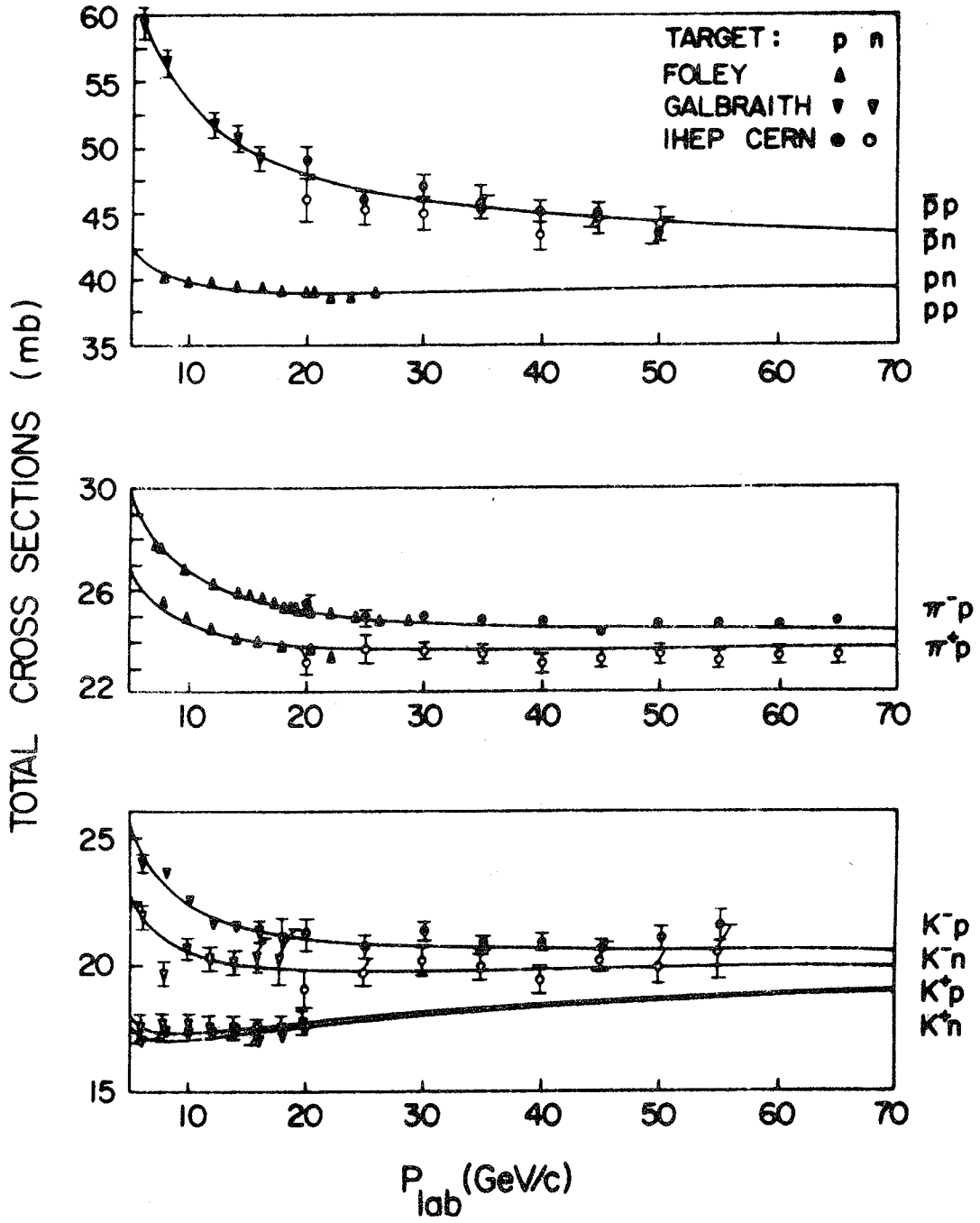
TOTAL CROSS SECTIONS (mb)
TARGET: p n
FOLEY ▲
GALBRAITH ▼ ▼
IHEP CERN ● ○
p̄p
p̄n
pn
pp
π⁻p
π⁺p
K⁻p
K⁻n
K⁺p
K⁺n
P_lab (GeV/c)

Fig:14

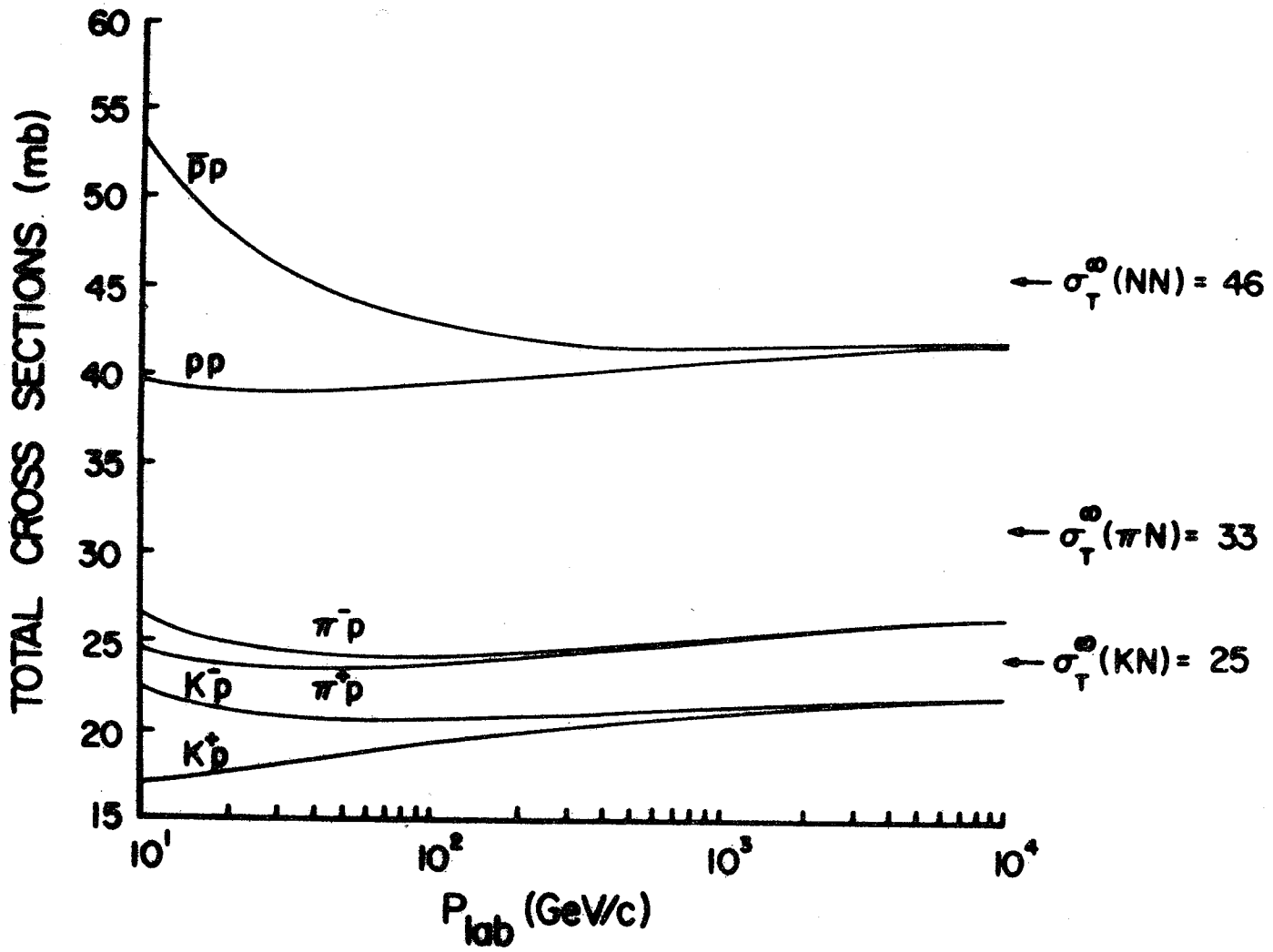
TOTAL CROSS SECTIONS (mb)
60
55
50
45
40
35
30
25
20
15
$\bar{p}p$
pp
$\pi^- p$
$K^- p$
$\pi^+ p$
$K^+ p$
$\leftarrow \sigma_T^{\infty}(NN) = 46$
$\leftarrow \sigma_T^{\infty}(\pi N) = 33$
$\leftarrow \sigma_T^{\infty}(KN) = 25$
10^1
10^2
10^3
10^4
P_{lab} (GeV/c)

Fig :15

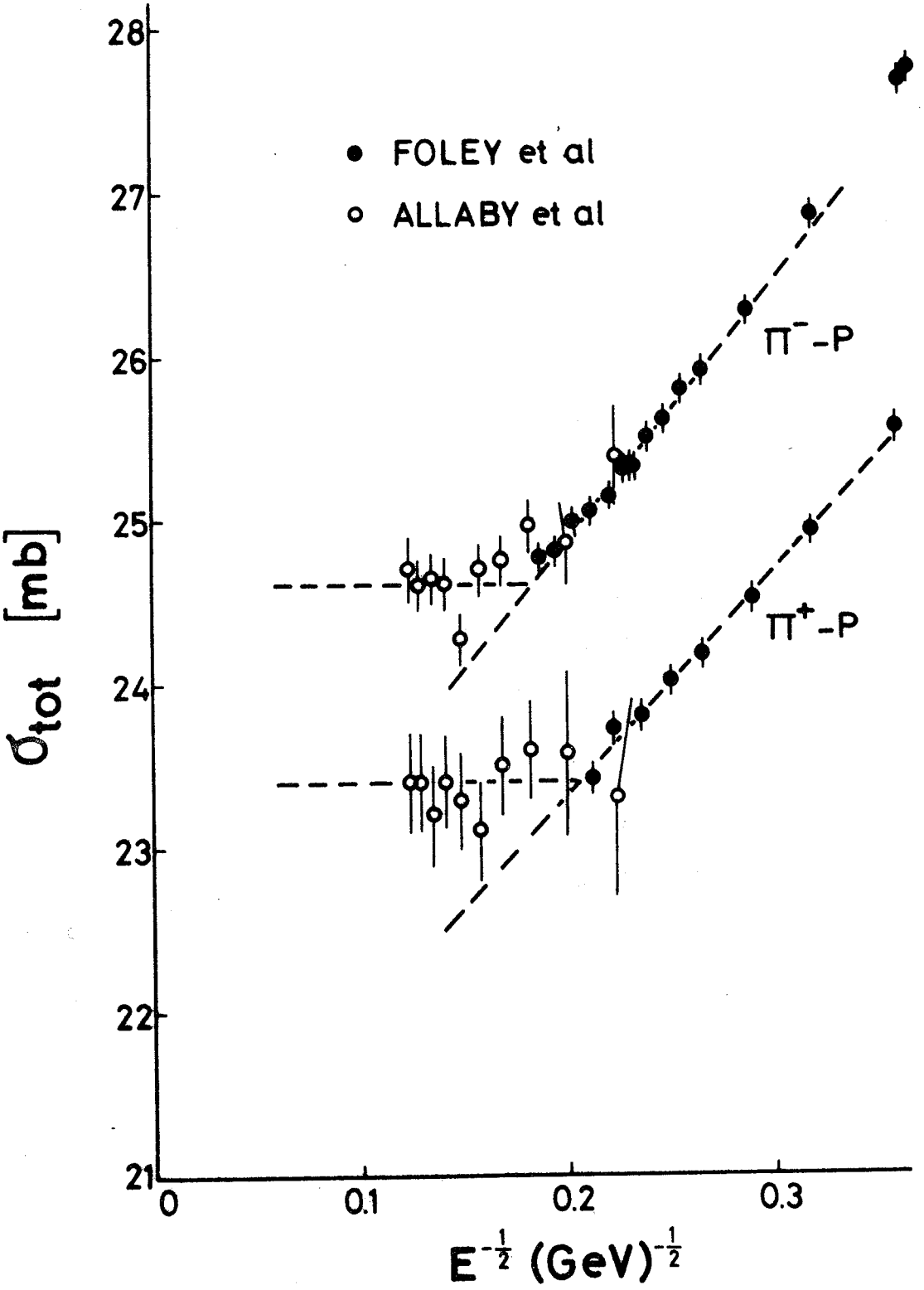
28
27
26
25
24
23
22
21
0
0.1
0.2
0.3
● FOLEY et al
○ ALLABY et al
π⁻-P
π⁺-P
σtot [mb]
E^-½ (GeV)^-½

Fig:16